UAV Collision Avoidance Utilizing ADS-B and TCAS with Independent Ranging

by

Andrea Henshall

A thesis submitted to the Graduate Faculty of
Auburn University
in partial fulfillment of the
requirements for the Degree of
Master of Science

Auburn, Alabama
August 4, 2018

Keywords: UAV, Collision Avoidance, ADS-B, TCAS

Approved by

Richard Chapman, Chair, Associate Professor of Computer Science and Software Engineering
Saad Biaz, Professor of Computer Science and Software Engineering
David Umphress, Professor of Computer Science and Software Engineering

Abstract

With the proliferation of Unmanned Aerial Vehicles (UAVs), their integration into the National Airspace System (NAS) is becoming increasingly imperative. To accomplish such integration, UAVs must be able to ”sense and avoid” other aerial vehicles. Automatic Dependent Surveillance-Broadcast (ADS-B) and Traffic Collision Avoidance Systems (TCAS) offer attractive data for use in estimating the relative position of an intruder aircraft. ADS-B will soon be mandatory in the NAS and its protocol permits independent range measurements in addition to the position and velocity estimates contained in messages. TCAS, while not mandatory for all aircraft, uses active interrogation of aircraft transponders - which are mandatory in a large portion of controlled airspace - to provide accurate range estimates to intruders. ADS-B reports, ADS-B independent ranges, and TCAS ranges were used as measurements to Extended Kalman Filters (EKFs) which provided estimates of the relative position and velocity of an intruder aircraft. Three EKF versions were examined: one with no delay states, one with position delay states to improve relative velocity estimates, and one with velocity delay states to estimate relative aircraft acceleration. The EKF with no delay states provided the most promising results to simulated encounters. When the process noise values were properly tuned, it provided improvements over un-processed ADS-B position and velocity values and performed well during periods of complete signal loss and random message loss.

Acknowledgments

First and foremost, I want to thank my partner, Ron, who has supported me in my endeavors from the day we met. Thank you for making the journey so much easier!

Thank you to Dr. Richard Chapman for being the first person at Auburn University to believe in my ability to succeed in this program. You offered support, guidance, and mentorship even before my first day of class.

I extend my thanks to the long list of faculty at Auburn University who always managed to find time to provide academic and professional advice despite their busy schedule, especially Dr. Xiao Qin and Dr. Saad Biaz.

Finally, thank you to my many friends and family members who contributed to and helped me celebrate moments of victory and offered unconditional love when I felt defeated. No one succeeds in a vacuum, and nothing I have today could have been gained without you.

Table of Contents

List of Figures

List of Tables

Chapter 1

Introduction

Unmanned Aerial Vehicles (UAVs) and Unmanned Aerial Systems (UASs) are becoming increasingly ubiquitous. They are utilized in military applications, in commercial delivery and photography, and by enthusiasts for recreational purposes. Regardless of one's personal thoughts on the above uses, UAVs have become a permanent fixture of modern life.

One of the principal concerns regarding UAV proliferation is the integration of UAVs with manned aircraft in increasingly congested airspace, especially near airports. For UAVs to be allowed to fly as close as they must to other aircraft in such airspace, they must have the ability to "sense and avoid" other aircraft. A variety of intruder aircraft detection methods and collision-avoidance algorithms have been explored. However, they tend to focus on the flight of UAVs in uncontrolled airspace: airspace in which aircraft may not need to strictly adhere to a given flight path and altitude. In controlled airspace, however, aircraft are not permitted to deviate from their assigned routes unless granted permission by the controlling authority or in the case of an emergency. Existing collision avoidance research frequently either advocates for early and large avoidance maneuvers which do not require precise determination of the intruder's location, or it utilizes dedicated detection systems which increase aircraft cost, weight, and complexity. The former solution would not be permitted in controlled airspace and the latter is not preferred. Ideally, intruder detection would be accomplished using equipment already required.

Automatic Dependent Surveillance-Broadcast (ADS-B) systems are of particular interest for intruder detection because they will soon be required equipment. ADS-B will be mandatory

for aircraft flying in controlled airspace in the United States by 2020 and the systems are in various stages of integration overseas. ADS-B messages contain a variety of useful data including the position and velocity of the transmitting aircraft along with error bounds for these values. Since ADS-B utilizes a pseudo-random, slotted transmission protocol and ADS-B position is Global Positioning System (GPS)-derived (which allows precise clock synchronization), receivers can estimate the propagation delay of the message and, by extension, the range to the transmitter. Existing research on the use of ADS-B for intruder position determination, however, does not examine the use of the signal itself to augment the reported position [1].

While existing Traffic Collision Avoidance Systems (TCAS) are another attractive option for UAV intruder detection, they are inadequate by themselves. First and foremost, the required equipment for TCAS use is not mandatory in all controlled airspace, therefore, TCAS would not always be able to provide collision avoidance guidance. Furthermore, TCAS only provides vertical deconfliction between two or more aircraft. Their ability to determine the bearing to an intruder aircraft is extremely poor. Aircraft close to the ground or near their service ceilings may not be able to maneuver vertically to avoid a collision, so vertical deconfliction capability alone is insufficient [2].

An attractive solution involves augmenting ADS-B reported parameters with range measurements from ADS-B and TCAS. Small systems already exist which include both ADS-B and TCAS. A properly tuned Extended Kalman Filter (EKF) can provide sufficient accuracy for UAVs to maneuver vertically or laterally away from other aircraft without violating Federal Aviation Regulations (FARs) for flying in controlled airspace. Furthermore, the cost of implementing such a system is marginally higher than only including the mandatory ADS-B components.

Chapter 2

Automatic Dependent Surveillance-Broadcast

Broadly, there are two types of ADS-B systems: those which utilize 978 MHz Universal Access Transceivers (UATs) and those which utilize 1090 MHz Mode-S transponders with Extended Squitter (1090ES). In addition to ADS-B messages, both systems support Traffic Information Services-Broadcast (TIS-B). TIS-B includes traffic information from non-ADS-B sources including ground-based radar systems. UATs support additional broadcast services to include Flight Information Services-Broadcast (FIS-B). FIS-B includes Notice to Airmen messages (NOTAMs), Temporary Flight Restrictions (TFRs), and a variety of weather information. The following algorithms are appropriate for either ADS-B system, however, simulations were conducted using the specifications for UATs due to their additional capabilities. The information contained in this document is for UATs unless otherwise noted.

UAT messages come in two broad types: ADS-B and ground uplink. Ground uplink messages include FIS-B messages. TIS-B messages can also be broadcast as ground uplink messages, however, it is preferred that they be transmitted as ADS-B messages. ADS-B messages are not limited to aerial vehicles; they can also be broadcast by surface vehicles and fixed or slowly moving obstacles.

UAT messages are transmitted using a combination of random-access and time-slots. A UAT frame is the basic unit used for time-slotting. It is one second long, begins at the start of each Coordinated Universal Time (UTC) second, and contains 3952 Message Start Opportunities (MSOs). MSOs occur every 250 μs with the first immediately following a 6 ms guard period at the start of the UAT frame. The last MSO occurs just before the final 6 ms guard period. Messages can only be transmitted at an MSO and during their corresponding segment:

ground or ADS-B. The ground segment is 176 ms long and is divided into 32 slots (a ground message will be transmitted at an MSO, but the length of the message will cover multiple MSOs). The ADS-B segment is 800 ms long and divided into 3200 slots (one for each MSO). A transmitter wishing to send an ADS-B message selects the MSO it will use based on a formula related to its position and the last MSO it used. This formula can be found in RTCA DO-282B. A 12 ms guard time is incorporated between the ground and ADS-B segments. A graphical representation of the UAT frame can be found in figure 2.1 [1].

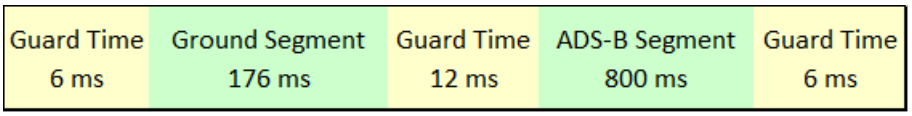

Figure 2.1: UAT Frame

To ensure UAT users are able to receive messages from 1090ES users and vice versa, ground transceivers are utilized. These ground stations receive both frequencies and formats of ADS-B messages and re-transmit them using the other frequency and format. These retransmitted messages are referred to as ADS-R (rebroadcast) messages. The maximum time between the reception of an ADS-B message and the transmission of the corresponding ADS-R message is 1 second. Ground stations also linearly extrapolate the horizontal position in the ADS-B message to compensate for the retransmission delay (within 100 ms). In lieu of accepting the latency of ADS-R messages or for operation in places in which such ground stations are not available, dual-frequency UATs can be utilized [3].

2.1 ADS-B Message Types

ADS-B messages consist of a 36 bit synchronization code, either 144 or 272 bits of payload (ADS-B basic versus ADS-B long messages) and 96 or 112 bits of forward error correction (FEC) parity bits. There are 32 different ADS-B message payload types, however, only seven are relevant to this research: ADS-B basic messages (type 0) and six types of ADS-B long messages.

All ADS-B messages start with four header (HDR) bytes and thirteen state vector (SV) bytes. The header contains the payload type code used to identify the message type, the address

qualifier which indicates what the address field represents, and the address field which is used to uniquely identify the message transmitter. The contents of the rest of the message depend on the message type, but may include mode status (MS), auxiliary state vector (AUX SV), target state (TS), trajectory change + 0 (TC + 0), and trajectory change + 1 (TC + 1). The basic message format consists of only the header and state vector. The long message formats contain more information. Fields labeled ”RES” are reserved for future use. The contents of each message type are summarized in table 2.1.

	Payload Byte Number				
Payload Type Code	1 - 4	5 - 17	18 - 24	25 - 29	30 - 34
0	HDR	SV	N/A*		
1	HDR	SV	MS		AUX SV
2	HDR	SV	RES		AUX SV
3	HDR	SV	MS		TS
4	HDR	SV	TC + 0		TS
5	HDR	SV	TC + 1		AUX SV
6	HDR	SV	RES	TS	AUX SV
*Byte 18 is reserved for future definition					

Table 2.1: ADS-B Payload Compositions

2.1.1 State Vector Element

Of particular interest are the contents of the state vector which can be found in table 2.2. The precise representation of the components of the state vector are beyond the scope of this thesis, but can be found in RTCA DO-282B. The encoding of TIS-B and ADS-R state vectors is identical to that of ADS-B messages with the exception that the last four bits are used to encode the TIS-B site ID rather than uplink feedback and the UTC bit is not used for TIS-B.

State Vector Composition (B = Broadcast; R = Rebroadcast)		
Description	Notes	Precision
Latitude	WGS-84	$2/2^{25}$ deg
Longitude	WGS-84	$2/2^{25}$ deg
Altitude Type	Geometric or pressure	
Altitude	Feet	12.5 ft
Navigation Integrity Category	Kilometers or meters	
Air/Ground State	Plus sub/supersonic indicator	
Reserved		
Horizontal Velocity	Knots	1/2 or 2 kts (supersonic)
Vertical Speed*	Feet per minute	32 ft/min
Coordinated Universal Time (UTC)	Coupled/uncoupled (not TIS-B)	
Uplink Feedback (B)	Ground messages/32 seconds	
TIS-B Site ID (R/TIS)		
*Plus source and sign; aircraft size when on the ground		

Table 2.2: State Vector Composition

2.1.2 Mode Status Element

The composition of the mode status element is shown in table 2.3 [1].

Mode Status Element	
Description	Notes
Emitter Category/Call Sign/Flight Plan ID	Type (heavy, rotor, etc.)
Emergency/Priority Status	Emergency/medical/etc.
UAT MOPS version	RTCA DO-282A/B
Source Integrity Level	SIL
Transmit Message Start Opportunity	6 LSBs of MSO
System Design Assurance	SDA
Navigation Accuracy Category for Position	NACp
Navigation Accuracy Category for Velocity	NACv
Barometric Altitude Integrity Code	NICbaro
Capability codes	UAT/1090ES in; TCAS/ACAS Operational (RA)
Operational Modes	RA/Ident active; Receiving ATC services
Call Sign Identification Flag	CSID (Contents of element 1)
Source Integrity Level Supplement	SILsupp (per hour/sample)
Geometric Vertical Accuracy	GVA
Single Antenna Flag	
Navigational Integrity Category Supplement	NICsupp

Table 2.3: Mode Status Composition

When a UAV receives a mode status element, it should consider several components. The emitter category should be evaluated as it can be used to determine the appropriate amount of lateral and vertical separation a UAV should maintain. The FARs and the Aeronautical Information Manual (AIM) published by the Federal Aviation Administration (FAA) provide separation guidance. The emitter category can also be used to determine whether or not the transmitting aircraft has the right of way. The FAA specifies the order of right of way for various aircraft (generally, less maneuverable aircraft over more maneuverable). Current FAA guidance should be consulted for specifics [4] [5]. The emergency/priority status should be

used to determine whether or not a UAV should expect to yield to the intruder (e.g. emergency and medical flights have traffic priority while aircraft declaring minimum fuel do not).

The Minimum Operational Performance Standards (MOPS) version is important in that it helps define the capabilities of the aircraft. Aircraft conforming to RCTA DO-282A have the 1090ES and do not have FIS-B capabilities while aircraft conforming to RTCA DO-282B have UATs which include the ability to receive FIS-B messages.

The SIL is defined as "the probability of reported horizontal position exceeding the radius of containment defined by the NIC without an alert, assuming there are no avionics faults [1]." SDA essentially describes the likelihood of transmitting aircraft sending false information. NACp and NACv are for 95% horizontal accuracy bounds. NICBaro indicates whether or not the barometric altitude being reported has been crossed checked and found consistent with another source of pressure altitude (if based on a Gilham code input) or not. These numbers should be evaluated by the receiving UAV to help define the "bubble" around the transmitting aircraft which the UAV should not penetrate [1].

The capabilities element can be used to determine whether or not an intruder aircraft can be expected to cooperate in a collision avoidance maneuver (e.g. if they have TCAS II with Resolution Advisory (RA) capabilities, the two systems will cooperate to de-conflict the vertical collision avoidance maneuvers of the two aircraft). Operational mode should alert a receiving aircraft to a temporary limiting condition of the transmitting aircraft (e.g. aircraft in the middle of responding to an RA may have limited ability to respond to a second conflict) [6].

SILsupp indicates if the SIL is measured on a per hour or per sample basis. GVA is for a 95% figure of merit (FOM). Single antenna aircraft have slightly different transmission schedules than dual-antenna aircraft (see section 2.2). The NICsupp flag augments the NIC encoding. These components could, again, be used to determine an appropriate avoidance bubble around the transmitting aircraft.

The NACp, NACv, and GVA values area shown in tables 2.4, 2.5, and 2.6. These values will be used in the EKF measurement covariance matrix which will be discussed in detail later.

NACp Encoding	
NACp	95% Horizontal Accuracy Bound
0	$\geq$ 18.52 km (10 NM)
1	$<$ 18.52 km (10 NM)
2	$<$ 7.408 km (4 NM)
3	$<$ 3.704 km (2 NM)
4	$<$ 1.852 km (1 NM)
5	$<$ 926 m (0.5 NM)
6	$<$ 555.6 m (0.3 NM)
7	$<$ 185.2 m (0.1 NM)
8	$<$ 92.6 m (0.05 NM)
9	$<$ 30 m
10	$<$ 10 m
11	$<$ 3 m
12 - 15	RES

Table 2.4: NACp Encoding

NACv Encoding	
NACv	95% Horizontal Error
0	$\geq$ 10 m/s
1	$<$ 10 m/s
2	$<$ 3 m/s
3	$<$ 1 m/s
4	$<$ 0.3 m/s
5 - 7	RES

Table 2.5: NACv Encoding

GVA Encoding	
GVA	95 Horizontal Error
0	< 150 m
1	≤ 150 m
2	≤ 45 m
3	RES

Table 2.6: GVA Encoding

2.1.3 Auxiliary State Vector Element

The auxiliary state vector consists of a secondary altitude measurement. It is the ”opposite” of the type in state vector altitude type field (barometric if the state vector has geometric and geometric if the state vector has barometric) and is encoded the same way as the altitude in the state vector.

2.1.4 Target State Element

Information in the target state element could be used to make an educated guess about what the transmitting aircraft will do next and provide better collision avoidance guidance. The target state element indicates the settings and status of either the Mode Control Panel (MCP) or the Flight Control Unit/Flight Management Unit (FCU/FMU). Either the MCP or the FCU/FMU can be coupled to an autopilot which will fly the programmed route/heading/altitude/airspeed/etc. A target state element indicating an intruder aircraft is on autopilot and flying a Vertical Navigation (VNAV) or Lateral Navigation (LNAV) approach, for instance, may be used to indicate to a UAV that it should select a climb over a descent and a turn away from known approach paths rather than toward them (if possible). Caution should be exercised when using the target state element for collision avoidance as there is no guarantee that the pilot will not override the autopilot and maneuver the aircraft unexpectedly. The contents of the target state element are summarized in table 2.7.

Target State Element		
Description	Notes	Value (precision)
Selected Altitude Type	SAT; MCP or FCU/FMS	0 or 1
Selected Altitude		(32 ft)
Barometric Pressure Setting	Minus 800 mb	(0.8 mb)
Heading Status	Valid or Invalid	1 or 0
Sign	Positive or Negative	0 or 1
Selected Heading	Degrees	180/256 deg
Status of MCP/FCU	Valid or Invalid	1 or 0
Autopilot Status	Engaged or Not	1 or 0
VNAV Status	Engaged or Not	1 or 0
Altitude Hold Status	Engaged or Not	1 or 0
Approach Mode	Engaged or Not	1 or 0
LNAV Status	Engaged or Not	1 or 0

Table 2.7: Target State Element

2.1.5 Trajectory Change Elements

Trajectory change elements (TC + 0 and TC + 1) have not yet been defined, but may offer additional opportunities for receiving aircraft to tailor their collision avoidance maneuvers. TC elements are intended to reveal what the transmitting aircraft intends to do in the near future. As with the target state element, there is no guarantee what is reported is what the transmitting aircraft will actually do.

2.2 ADS-B Message Scheduling

ADS-B message are transmitted by aircraft once per second, but the type of message sent and the antenna used (if a multi-antenna system) vary by aircraft classification and status. DO-282B has specific aircraft definitions, but general descriptions are provided below.

Payload Type Code Allocation				
Equipment Class	PS-A	PS-B	PS-C	PS-D
Most Aircraft/Surface Vehicles*	1	0	2	0
Aircraft/Vehicle with alternating tx*	3	6	0	6
Aircraft, dual-receive, med pwr tx*	1	4	4	4
Aircraft, dual-receive, high pwr tx*	1	4	5	4
Surface vehicle/obstacle*	1	0	0	0
*If Flight Plan ID, Emergency/Priority Status, or NICsup is changed, message types 1 or 3 will be transmitted for 6 consecutive seconds before resuming this schedule				

Table 2.8: ADS-B Payload Compositions

The Payload Selection (PS) identified above is transmitted on the following schedule for dual-transmitters (single transmitters will simply transmit PS A-D except as noted in table 2.8) [1]:

Message Transmission Cycle																
Antenna:	T	T	B	B	T	T	B	B	T	T	B	B	T	T	B	B
PS:	A	B	C	D	D	A	B	C	C	D	A	B	B	C	D	A
Second:	1	2	3	4	5	6	7	8	9	10	11	12	13	14	15	16

Table 2.9: ADS-B Payload Compositions

2.3 ADS-B Accuracy Requirements

The accuracy requirements for ADS-B data used in collision avoidance applications have yet to be defined. There are, however, accuracy requirements for other purposes. Table 2.10 outlines the minimum requirements for other applications which can reasonably be assumed to require less precision than collision avoidance applications. The position and velocity requirements are derived from requirements for delegated separation: operations in which responsibility for

maintaining adequate separation between aircraft is transferred in whole or in part from Air Traffic Control (ATC) to participating aircraft. The altitude requirement is taken from the requirements for ATC surveillance: operations in which ATC uses ADS-B rather than radar to provide traffic services [2]. These were the values used for the EKF measurement covariance matrix.

ADS-B Minimum Requirements	
Parameter	0.95 Metric (Parameter Value)
Position	$\leq$ 30 m ($\geq$ 9 NACp)
Velocity	$\leq$ 1 m/s ($\geq$ 3 NACv)
Altitude	$\leq$ 125 ft (N/A)

Table 2.10: ADS-B Minimum Requirements

Chapter 3

Traffic Collision Avoidance System

TCAS I and II (or ACAS: Airborne Collision Avoidance System) are the primary systems currently in use for airborne traffic situational awareness and collision avoidance. TCAS uses interrogations of transponder-equipped aircraft within a given range to provide traffic situational awareness to aircrew. Traffic is often visually displayed in the cockpit on a map fixed relative to the ownship with traffic displayed at relative distances and approximate bearings from the ownship symbol. If an intruder meets certain collision potential criteria (which is dependent upon a number of factors), a Traffic Alert (TA) is generated. A TA is usually indicated by an aural alert and the intruder's track being highlighted on the TCAS display. TCAS II provides additional capabilities. If an intruder meets the threshold for high likelihood of collision (which is, again, situation dependent), the system issues a Resolution Advisory (RA): vertical avoidance recommendations often in the form of both aural instructions and visual cues.

The type of alert provided by TCAS depends on the type of TCAS used and the equipment installed on the intruder aircraft. TCAS I systems can only generate TAs for intruder aircraft regardless of the type of transponder on the intruder. TCAS II can generate RAs for aircraft equipped with mode-C or mode-S transponders, but can only generate TAs for those using mode-A transponders. Mode-A transponders only transmit the four-digit octal code or "squawk" code assigned by ATC. By contrast, mode-C transponders transmit both the aircraft's squawk code and pressure altitude, allowing for vertical avoidance recommendations. Mode-S transponders transmit additional information utilized by TCAS II to provide coordinated maneuvers if the intruder aircraft is also equipped with TCAS II. When two aircraft equipped with TCAS II and functional mode-S transponders meet the threshold for an RA, the systems will

ensure the vertical maneuver recommended to one aircraft does not conflict with the recommendation given to the other (e.g. one will be commanded to climb while the other to maintain altitude or descend). A chart of the levels of protection provided by combinations of systems can be found in figure 3.1.

		Own Aircraft Equipment	
		TCAS I	**TCAS II**
Target Aircraft Equipment	Mode A XPDR ONLY	TA	TA
	Mode C or Mode S XPDR	TA	TA and Vertical RA
	TCAS I	TA	TA and Vertical RA
	TCAS II	TA	TA and Coordinated Vertical RA

Figure 3.1: TCAS Levels of Protection

On the surface, TCAS seems like the ideal system to use for UAV collision avoidance, however, there are drawbacks. The first issue is that mode-C transponders are not required in all controlled airspace. A UAV cannot vertically maneuver to avoid another aircraft if it does not know the altitude of the intruder. Even if mode-C were to be required in all controlled airspace, TCAS can only provide accurate vertical data on tracked aircraft; it may not have accurate (or any) bearing data. The lack of accurate bearing data precludes horizontal avoidance maneuvers. In congested airspace, near an aircraft's ceiling, and near the ground, it may not be possible for an aircraft to maneuver vertically to avoid a collision. Another solution is required. [6].

Chapter 4

Previous Research

There are a multitude of publications on the use of ADS-B for UAV collision avoidance. Katta and Madani [7] produced a paper on the use of reported ADS-B position for collision avoidance. Like many others, Katta and Madani advocated for early aircraft collision avoidance maneuvers which resulted in large deviations from the original paths. Ramasamy and Sabatini discussed a general approach to processing multiple sources of information about intruder aircraft positions including ADS-B, TCAS, Synthetic Aperture Radar (SAR), cameras, and other sources. They used a Boolean-logic-based decision tree for potential collision detection, but did not address combining sensor data to estimate the intruder's trajectory [8].

RTCA DO-300A describes the requirements for a hybrid surveillance system of 1090ES ADS-B and TCAS. The purpose of using the system as described in DO-300A, however, is to reduce the number of active interrogations of an intruder's transponder rather than improve intruder position estimates. Data from the two systems are not combined, instead ADS-B reports are used in lieu of TCAS interrogations for distant intruders, TCAS is used to validate ADS-B position reports for intermediate intruders, and proximate intruders are tracked using TCAS interrogations only [2].

RTCA DO-282B discusses how the primary objective of the timing requirements for the transmission and reception of ADS-B messages is to support independent range measurements between the transmitter and receiver. However, the purpose of such independent range measurements is to validate ADS-B reported positions, decreasing the likelihood of erroneous or spoofed data being accepted as accurate. There is no discussion on the use of the estimated range to augment the reported position [1]. No publications were found which discussed the

use of ADS-B signal propagation delay to augment the ADS-B reported position. Yang, Strader, Gu, and Hypes, however, discussed the use of cooperative UAV ranging for a group of UAVs in formation [9]. Their method of incorporating range measurements between cooperating UAVs into an EKF for position estimation was very similar to that used in the EKFs described below.

As this work focused on intruder position estimation and not avoidance maneuvers, methods for collision avoidance maneuver determination, execution, and post-maneuver path-determination were not addressed.

Chapter 5

Kalman Filters

The Kalman filter is a popular estimation tool. It provides a formulation for the minimum mean-square error (MMSE) problem for systems with multiple inputs and multiple outputs. The Linear, Time-Invariant (LTI) version provides optimal state estimates if the optimal gain (the Kalman gain) is utilized. Other versions of the Kalman filter can take into account time-varying parameters, non-linear processes or observation functions, and correlated measurement and process noise.

For this research, the EKF and EKF with position and velocity delay states were considered and evaluated. EKFs which included range and/or range rate as states were considered as variations. For these EKFs, the state transition equations were non-linear, the state transition matrices and process covariance matrices were time-dependent, and the state covariance matrix was excessively complicated. For these reasons, the models were abandoned before any useful results were produced.

5.1 The Extended Kalman Filter

Since the relative position and rate of closure of the distance between a UAV and an intruder aircraft was desired, the states selected for the EKF were relative position and velocity in three dimensions. Any ADS-B and TCAS data which provided information related to these states were used as measurements: reported horizontal position and velocity, one or two reported altitude measurements, reported vertical speed, and ADS-B and TCAS range estimates. Both the ADS-B and TCAS range estimates included some bias incurred through errors in time-stamping signals and data processing. Since the Kalman filter treats process and measurement

noise as zero-mean, TCAS and ADS-B range biases had to be included as states. The Kalman filter state vector was then:

$$x = \begin{bmatrix} Bias_{TCAS} \\ Bias_{ADS-B} \\ E \\ \dot{E} \\ N \\ \dot{N} \\ U \\ \dot{U} \end{bmatrix} \tag{5.1}$$

For which E is the difference between the intruder aircraft and UAV east positions and $\dot{E}$ is the rate of change of this value. N is the difference in north position and U is the difference in altitude (up). All states are in units of meters and meters per second.

As previously described, the measurements were:

$$z = \begin{bmatrix} r_{TCAS} \\ r_{ADS-B} \\ E \\ \dot{E} \\ N \\ \dot{N} \\ U_{baro} \\ U_{geometric} \\ \dot{U} \end{bmatrix} \tag{5.2}$$

Again, all values were in meters or meters per second. Since the ADS-B state vector contained the transmitter's position in latitude and longitude, these values were converted to a local coordinate frame (East, North, and Up) prior to being used by the Kalman filter. There are a wide variety of conversion algorithms of varying levels of complexity which induce errors

ranging from millimeters (spherical harmonics) to over 100 m (simple equations with look-up tables for various parameters). For this thesis, it was assumed the reported position data was pre-processed in such a way as to incur negligible errors. Using a different conversion method may require the errors be accounted for in the covariance matrices.

5.1.1 Projection Equations

A continuous process for which there is no deterministic input and no modeled coupling between stochastic inputs and measurements (like this system) can be represented by the following system of equations:

$$\begin{aligned} \dot{x} &= Ax + w \\ y &= Cx + v \end{aligned} \tag{5.3}$$

For which x is the state vector, A is the continuous process dynamics matrix, w is the continuous process noise vector, y is the output vector, and v is the continuous measurement noise vector. Since the filter receives discrete measurements, a discrete model must be used which takes the form:

$$\begin{aligned} x_{k+1} &= \Phi x_k + w_k \\ y_k &= H x_k + v_k \end{aligned} \tag{5.4}$$

For which k is the sample time, Φ is the state transition matrix, and H is the discrete model observation matrix.

For this version of the Kalman filter, the process and measurement noise is uncorrelated. The noise is also uncorrelated with previous states since it is Gaussian:

$$\begin{aligned} E[v_k] &= 0 \\ E[v_k w_{k+1}^T] &= 0 \\ E[x_k v_{k+1}^T] &= 0 \\ E[x_k w_{k+1}^T] &= 0 \\ E[w_k] &= 0 \end{aligned} \tag{5.5}$$

The process and measurement covariance matrices are defined as:

$$\begin{aligned} R_k &= E[v_k v_k^T] \\ Q_k &= E[w_k w_k^T] \end{aligned} \tag{5.6}$$

Normally, the Kalman filter linearizes a model around some nominal "trajectory". Since no such trajectory was utilized, this version of the Kalman filter is referred to as an Extended Kalman Filter. The EKF essentially uses the previous state estimate as the starting point from which to estimate the current state's "deviation" rather than a point on a nominal trajectory. If the previous estimate is poor, the updated estimate will be poor. For this reason, the EKF may not converge in some circumstances such as when there is a large amount of uncertainty in the initial state or measurement errors are large. Despite this drawback, it is still the gold standard for applications like Global Positioning Systems (GPS) [10].

To develop the discrete model for this system, the continuous state space model was considered. For each direction, there was a position and rate term which took the form:

$$\begin{bmatrix} \dot{s} \\ \ddot{s} \end{bmatrix} = \begin{bmatrix} 0 & 1 \\ 0 & 0 \end{bmatrix} \begin{bmatrix} s \\ \dot{s} \end{bmatrix} \tag{5.7}$$

For which s is distance and:

$$A = \begin{bmatrix} 0 & 1 \\ 0 & 0 \end{bmatrix} \tag{5.8}$$

The solution to this differential equation is easily seen to be an exponential of Euler's number. The continuous process dynamics matrix was converted to the discrete state transition matrix by taking $\Phi(t_k, t_{k+1}) = e^{A\Delta t}$. Taking the Taylor series expansion of $e^{A\Delta t}$, yielded $I + A\Delta t$ (the remaining terms were zero) which equals:

$$\Phi = \begin{bmatrix} 1 & \Delta t \\ 0 & 1 \end{bmatrix} \tag{5.9}$$

Clearly, the relationship between the discrete measurement noise vector and the continuous is simply:

$$w_k = \int_{t_k}^{t_{k+1}} \Phi(t_{k+1}, \tau) w(\tau) d\tau \tag{5.10}$$

This means the process covariance matrix is:

$$Q_k = E\left[\left[\int_{t_k}^{t_{k+1}} \Phi(t_{k+1}, \tau) w(\tau) d\tau\right]\left[\int_{t_k}^{t_{k+1}} \Phi(t_{k+1}, \eta) w^T(\eta) d\eta\right]^T\right] \tag{5.11}$$

Which becomes:

$$Q_k = \int_{t_k}^{t_{k+1}} \int_{t_k}^{t_{k+1}} \Phi(t_{k+1}, \tau) E[w(\tau) w^T(\eta)] \Phi^T(t_{k+1}, \eta) d\tau d\eta \tag{5.12}$$

For which $E[w(\tau)w^T(\eta)]$ is a matrix of Dirac delta functions which are known from the continuous model. The covariance matrix can then be written as:

$$Q_k = \int_{t_k}^{t_{k+1}} \Phi(t_{k+1}, \tau) N \Phi^T(t_{k+1}, \tau) d\tau \tag{5.13}$$

For which $N = E[ww^T]$

For this process, the only "noise" was any unaccounted for acceleration between the UAV and the intruder aircraft. Therefore:

$$N_S = \begin{bmatrix} 0 & 0 \\ 0 & n_{\dot{s}} \end{bmatrix} \tag{5.14}$$

For which the diagonal terms are the variances of the respective states per unit of time and $n_{\dot{s}} = E[e_{\dot{s}}]$ is the expected value of the noise in the velocity term caused by not accounting for the relative acceleration between the two aircraft in the model. A model described later includes an acceleration term.

The process covariance matrix for each direction is then:

$$Q_S = n_{\dot{S}} \begin{bmatrix} \frac{\Delta t^3}{3} & \frac{\Delta t^2}{2} \\ \frac{\Delta t^2}{2} & \Delta t \end{bmatrix} \tag{5.15}$$

The bias terms are constant, so projected states are simply equal to the updated states of the previous time period. Furthermore, there is no process noise since they are constant terms and modeled as such. The complete state transition matrix was then:

$$\Phi = \begin{bmatrix} 1 & 0 & 0 & 0 & 0 & 0 & 0 & 0 \\ 0 & 1 & 0 & 0 & 0 & 0 & 0 & 0 \\ 0 & 0 & 1 & \Delta t & 0 & 0 & 0 & 0 \\ 0 & 0 & 0 & 1 & 0 & 0 & 0 & 0 \\ 0 & 0 & 0 & 0 & 1 & \Delta t & 0 & 0 \\ 0 & 0 & 0 & 0 & 0 & 1 & 0 & 0 \\ 0 & 0 & 0 & 0 & 0 & 0 & 1 & \Delta t \\ 0 & 0 & 0 & 0 & 0 & 0 & 0 & 1 \end{bmatrix} \tag{5.16}$$

The process covariance matrix in 2x2 block format was:

$$Q = \begin{bmatrix} 0 & 0 & 0 & 0 \\ 0 & Q_E & 0 & 0 \\ 0 & 0 & Q_N & 0 \\ 0 & 0 & 0 & Q_U \end{bmatrix} \tag{5.17}$$

The projection of the previous state estimate to the current time period is accomplished via:

$$\hat{x}_k^- = \Phi \hat{x}_{k-1}^+ \tag{5.18}$$

For which the hat represents an estimated value, the superscript minus means prior to the measurement update, and the superscript plus means after the measurement update.

To keep track of the estimated error envelopes for each of the states throughout the process of projecting and updating the states, the state covariance matrix is used which is defined as:

$$P_k^- = E[e_k^- e_k^{-T}] \tag{5.19}$$

For which $e_k^- = x_k - \hat{x}_k^-$. The covariance matrix is updated after a projection by:

$$P_k^- = \Phi P_{k-1}^+ \Phi^T + Q_{k-1} \tag{5.20}$$

5.1.2 Measurement Update Equations

To update the state estimates when provided with one or more measurements, essentially an educated guess is made about what the measurements are - based on the projection of previously updated states to the current time - and compared to the actual measurements. The difference between the two is weighted relative to the current state estimate via the Kalman gain and used to update said estimate. The equation for accomplishing this update is:

$$\hat{x}_k^+ = \hat{x}_k^- + K_k(z_k - \hat{z}_k) \tag{5.21}$$

For an LTI Kalman filter, the measurement estimate is computed using the observation matrix such that:

$$\hat{z}_k = H_k \hat{x}_k^- \tag{5.22}$$

Clearly, observation matrix, H, relates the states linearly to the measurements. The relationship between the position and velocity states to their respective measurements was simple to represent: the states were equal to their measurements. The TCAS and ADS-B range measurements, however, were non-linearly related to the states:

$$\begin{aligned} r_{TCAS} &= Bias_{TCAS} + \sqrt{E^2 + N^2 + U^2} \\ r_{ADS-B} &= Bias_{ADS-B} + \sqrt{E^2 + N^2 + U^2} \end{aligned} \tag{5.23}$$

Calculating the estimated measurements ($\hat{z}$) given the state estimate was still simple, however, the observation equations had to be linearized in order to get the observation matrix. This was accomplished by taking the Jacobian of the measurements with respect to the states evaluated at the previous time step ($\hat{x}_{k-1}^{+}$):

$$\frac{\partial h}{\partial x} = \begin{bmatrix} \frac{\partial h_1}{\partial x_1} & \frac{\partial h_1}{\partial x_2} & \dots \\ \frac{\partial h_2}{\partial x_1} & \frac{\partial h_2}{\partial x_2} & \dots \\ \vdots & \vdots & \ddots \end{bmatrix}_{\hat{x}_{k-1}^{+}} \tag{5.24}$$

For this system:

$$H = \begin{bmatrix} 1 & 0 & \frac{\partial r_{TCAS}}{\partial E} & 0 & \frac{\partial r_{TCAS}}{\partial N} & 0 & \frac{\partial r_{TCAS}}{\partial U} & 0 \\ 0 & 1 & \frac{\partial r_{ADS-B}}{\partial E} & 0 & \frac{\partial r_{ADS-B}}{\partial N} & 0 & \frac{\partial r_{ADS-B}}{\partial U} & 0 \\ 0 & 0 & 1 & 0 & 0 & 0 & 0 & 0 \\ 0 & 0 & 0 & 1 & 0 & 0 & 0 & 0 \\ 0 & 0 & 0 & 0 & 1 & 0 & 0 & 0 \\ 0 & 0 & 0 & 0 & 0 & 1 & 0 & 0 \\ 0 & 0 & 0 & 0 & 0 & 0 & 1 & 0 \\ 0 & 0 & 0 & 0 & 0 & 0 & 1 & 0 \\ 0 & 0 & 0 & 0 & 0 & 0 & 0 & 1 \end{bmatrix}_{\hat{x}_{k-1}^{+}} \tag{5.25}$$

For which:

$$\begin{aligned} \frac{\partial r}{\partial Bias} &= 1 \\ \left.\frac{\partial r}{\partial S}\right|_{\hat{x}_{k-1}^{+}} &= \frac{\hat{S}_{k-1}^{+}}{\sqrt{(\hat{E}_{k-1}^{+})^2 + (\hat{N}_{k-1}^{+})^2 + (\hat{U}_{k-1}^{+})^2}} \end{aligned} \tag{5.26}$$

For which S represents any of the position states (E, N, or U). With the observation matrix, the Kalman gain is calculated via:

$$K_k = P_k^- H_k^T (H_k P_k^- H_k^T + R_k)^{-1} \tag{5.27}$$

The covariance matrix is updated via:

$$P_k^+ = (I - K_k H_k) P_k^- (I - K_k H_k)^T + K_k R_k K_k^T \tag{5.28}$$

To ensure useful data about each of the states is gained from the measurements, the observability of the system is checked. The rank of the observability matrix is equal to the number of linearly independent states that can be estimated. If the observation matrix is time-varying, the observability matrix is:

$$O = [H_k | H_{k+1}\Phi | H_{k+2}\Phi^2 | H_{k+3}\Phi^3 | \cdots | H_{k+n-1}\Phi^{n-1}] \tag{5.29}$$

For which n is the number of states. If the rank of the observability matrix is equal to n, all of the states are observable. A rank-deficient observation matrix does not necessarily mean the filter must be changed. Extended periods of missing measurements may cause a temporary lack of observability of some states. Other times, the rank-deficiency of the observability matrix indicates that some states are not observable by themselves, but their linear combination with other states may be observable. For the EKF described above and those described later, the ranks of the observability matrices with no missing measurements were equal to the number of states. This indicated that all of the states were observable in the presence of all measurements.

5.2 The Extended Kalman Filter with Position Delay States

In an effort to provide better state estimates, velocity and position delay states were considered. If measurements are retained from previous time steps and used to provide current measurements (e.g. integrals or derivatives) of states, the filter is referred to as a delayed-state filter. For such a filter, the measurement and process noise are no longer uncorrelated. It is beyond the scope of this thesis to derive the equations for such a filter. Instead, the revised recursive equations are simply listed below. Their derivations can be found in [10].

The states and the state transition matrix did not change, however, the measurements became:

$$z = \begin{bmatrix} r_{TCAS,k} \\ r_{ADS-B,k} \\ E_k \\ \dot{E}_k \\ \frac{E_k - E_{k-1}}{\Delta t} \\ N_{k1} \\ \dot{N}_{ADS-B,k} \\ \frac{N_k - N_{k-1}}{\Delta t} \\ U_{baro,k} \\ U_{geometric,k} \\ \dot{U}_{ADS_B} \\ \frac{U_{baro,k} - U_{baro,k-1}}{\Delta t} \\ \frac{U_{geometric,k} - U_{geometric,k-1}}{\Delta t} \end{bmatrix} \tag{5.30}$$

States 5, 8, 12, and 13 were essentially additional measurements of the relative velocity between the UAV and the intruder.

A new matrix, J, was added which related previous states to the current measurement. For this system, the J matrix was:

$$J = \begin{bmatrix} 0 & 0 & 0 & 0 & 0 & 0 & 0 & 0 \\ 0 & 0 & 0 & 0 & 0 & 0 & 0 & 0 \\ 0 & 0 & 0 & 0 & 0 & 0 & 0 & 0 \\ 0 & 0 & 0 & 0 & 0 & 0 & 0 & 0 \\ 0 & 0 & -1 & 0 & 0 & 0 & 0 & 0 \\ 0 & 0 & 0 & 0 & 0 & 0 & 0 & 0 \\ 0 & 0 & 0 & 0 & 0 & 0 & 0 & 0 \\ 0 & 0 & 0 & 0 & -1 & 0 & 0 & 0 \\ 0 & 0 & 0 & 0 & 0 & 0 & 0 & 0 \\ 0 & 0 & 0 & 0 & 0 & 0 & 0 & 0 \\ 0 & 0 & 0 & 0 & 0 & 0 & 0 & 0 \\ 0 & 0 & 0 & 0 & 0 & 0 & -1 & 0 \\ 0 & 0 & 0 & 0 & 0 & 0 & -1 & 0 \end{bmatrix} \tag{5.31}$$

The measurement estimate for a delayed-state filter is:

$$\hat{z}_k = H_k \hat{x}_k^- + J_k \hat{x}_{k-1}^+ \tag{5.32}$$

The Kalman gain is then:

$$K_k = [P_k^- H_k^T + \Phi_{k-1} P_{k-1}^+ J_k^T] L_k^{-1} \tag{5.33}$$

For which:

$$L_k = H_k P_k^- H_k^T + R_k + J_k P_{k-1}^+ \Phi_{k-1}^T H_k^T + H_k \Phi_{k-1} P_{k-1}^+ J_k^T + J_k P_{k-1}^+ J_k^T \tag{5.34}$$

The estimate update equation does not change, however, the covariance update becomes:

$$P_k^+ = P_k^- - K_k L_k K_k^T \tag{5.35}$$

5.3 The Extended Kalman Filter with Velocity Delay States

In an attempt to use the difference between successive velocity measurements to provide information about the relative acceleration between the UAV and an intruder aircraft, a version of the EKF was developed using velocity delay states. For this version, the state vector was:

$$x = \begin{bmatrix} Bias_{TCAS} \\ Bias_{ADS-B} \\ E \\ \dot{E} \\ \ddot{E} \\ N \\ \dot{N} \\ \ddot{N} \\ U \\ \dot{U} \\ \ddot{U} \end{bmatrix} \tag{5.36}$$

The measurement vector was:

$$z = \begin{bmatrix} r_{TCAS,k} \\ r_{ADS-B,k} \\ E_k \\ \dot{E}_k \\ \frac{\dot{E}_k - \dot{E}_{k-1}}{\Delta t} \\ N_k \\ \dot{N}_{ADS-B,k} \\ \frac{\dot{N}_k - \dot{N}_{k-1}}{\Delta t} \\ U_{baro,k} \\ U_{geometric,k} \\ \dot{U}_{ADS-B} \\ \frac{\dot{U}_k - \dot{U}_{k-1}}{\Delta t} \end{bmatrix} \tag{5.37}$$

The continuous model was then:

$$\begin{bmatrix} \dot{s} \\ \ddot{s} \\ \dddot{s} \end{bmatrix} = \begin{bmatrix} 0 & 1 & 0 \\ 0 & 0 & 1 \\ 0 & 0 & 0 \end{bmatrix} \begin{bmatrix} s \\ \dot{s} \\ \ddot{s} \end{bmatrix} \tag{5.38}$$

For which:

$$A = \begin{bmatrix} 0 & 1 & 0 \\ 0 & 0 & 1 \\ 0 & 0 & 0 \end{bmatrix} \tag{5.39}$$

With the addition of the acceleration term, the state transition matrix and process covariance matrices were re-calculated using the process described in section 5.1.1. Following this procedure, the state transition matrix was:

$$\Phi = \begin{bmatrix} 1 & 0 & 0 & 0 & 0 & 0 & 0 & 0 & 0 & 0 & 0 \\ 0 & 1 & 0 & 0 & 0 & 0 & 0 & 0 & 0 & 0 & 0 \\ 0 & 0 & 1 & \Delta t & \frac{\Delta t^2}{2} & 0 & 0 & 0 & 0 & 0 & 0 \\ 0 & 0 & 0 & 1 & \Delta t & 0 & 0 & 0 & 0 & 0 & 0 \\ 0 & 0 & 0 & 0 & 1 & & 0 & 0 & 0 & 0 & 0 \\ 0 & 0 & 0 & 0 & 0 & 1 & \Delta t & \frac{\Delta t^2}{2} & 0 & 0 & 0 \\ 0 & 0 & 0 & 0 & 0 & 0 & 1 & \Delta t & 0 & 0 & 0 \\ 0 & 0 & 0 & 0 & 0 & 0 & 0 & 1 & 0 & 0 & 0 \\ 1 & 0 & 0 & 0 & 0 & 0 & 0 & 0 & 1 & \Delta t & \frac{\Delta t^2}{2} \\ 1 & 0 & 0 & 0 & 0 & 0 & 0 & 0 & 0 & 1 & \Delta t \\ 1 & 0 & 0 & 0 & 0 & 0 & 0 & 0 & 0 & 0 & 1 \end{bmatrix} \tag{5.40}$$

The continuous process covariance matrix was:

$$N_S = \begin{bmatrix} 0 & 0 & 0 \\ 0 & 0 & 0 \\ 0 & 0 & n_{\ddot{s}} \end{bmatrix} \tag{5.41}$$

The discrete process covariance matrix for each direction was:

$$Q_S = n_{\ddot{S}} \begin{bmatrix} \frac{\Delta t^5}{20} & \frac{\Delta t^4}{8} & \frac{\Delta t^3}{6} \\ \frac{\Delta t^4}{8} & \frac{\Delta t^3}{3} & \frac{\Delta t^2}{2} \\ \frac{\Delta t^3}{6} & \frac{\Delta t^2}{2} & \Delta t \end{bmatrix} \tag{5.42}$$

The entire process covariance matrix took the same block format as in section 5.1.1 with the zero blocks appropriately sized to fill in the off-diagonals.

The observation matrix became:

$$H = \begin{bmatrix} 1 & 0 & \frac{\partial r_{TCAS}}{\partial E} & 0 & 0 & \frac{\partial r_{TCAS}}{\partial N} & 0 & 0 & \frac{\partial r_{TCAS}}{\partial U} & 0 & 0 \\ 0 & 1 & \frac{\partial r_{ADS-B}}{\partial E} & 0 & 0 & \frac{\partial r_{ADS-B}}{\partial N} & 0 & 0 & \frac{\partial r_{ADS-B}}{\partial U} & 0 & 0 \\ 0 & 0 & 1 & 0 & 0 & 0 & 0 & 0 & 0 & 0 & 0 \\ 0 & 0 & 0 & 1 & 0 & 0 & 0 & 0 & 0 & 0 & 0 \\ 0 & 0 & 0 & 1 & 0 & 0 & 0 & 0 & 0 & 0 & 0 \\ 0 & 0 & 0 & 0 & 0 & 1 & 0 & 0 & 0 & 0 & 0 \\ 0 & 0 & 0 & 0 & 0 & 0 & 1 & 0 & 0 & 0 & 0 \\ 0 & 0 & 0 & 0 & 0 & 0 & 1 & 0 & 0 & 0 & 0 \\ 0 & 0 & 0 & 0 & 0 & 0 & 0 & 0 & 1 & 0 & 0 \\ 0 & 0 & 0 & 0 & 0 & 0 & 0 & 0 & 1 & 0 & 0 \\ 0 & 0 & 0 & 0 & 0 & 0 & 0 & 0 & 0 & 1 & 0 \\ 0 & 0 & 0 & 0 & 0 & 0 & 0 & 0 & 0 & 1 & 0 \end{bmatrix} \tag{5.43}$$

The J matrix was then [10]:

$$J = \begin{bmatrix} 0 & 0 & 0 & 0 & 0 & 0 & 0 & 0 & 0 & 0 & 0 \\ 0 & 0 & 0 & 0 & 0 & 0 & 0 & 0 & 0 & 0 & 0 \\ 0 & 0 & 0 & 0 & 0 & 0 & 0 & 0 & 0 & 0 & 0 \\ 0 & 0 & 0 & 0 & 0 & 0 & 0 & 0 & 0 & 0 & 0 \\ 0 & 0 & 0 & -1 & 0 & 0 & 0 & 0 & 0 & 0 & 0 \\ 0 & 0 & 0 & 0 & 0 & 0 & 0 & 0 & 0 & 0 & 0 \\ 0 & 0 & 0 & 0 & 0 & 0 & 0 & 0 & 0 & 0 & 0 \\ 0 & 0 & 0 & 0 & 0 & 0 & -1 & 0 & 0 & 0 & 0 \\ 0 & 0 & 0 & 0 & 0 & 0 & 0 & 0 & 0 & 0 & 0 \\ 0 & 0 & 0 & 0 & 0 & 0 & 0 & 0 & 0 & 0 & 0 \\ 0 & 0 & 0 & 0 & 0 & 0 & 0 & 0 & 0 & 0 & 0 \\ 0 & 0 & 0 & 0 & 0 & 0 & 0 & 0 & 0 & -1 & 0 \end{bmatrix} \tag{5.44}$$

Chapter 6

Simulation

To test the above Kalman filters, a Matlab simulation environment was created. Through a ”driver” program, a user could select the type of Kalman filter to use, UAV and intruder trajectory characteristics, measurement and process noise values, measurement loss characteristics, range bias values, and ADS-B message characteristics.

For the simulations performed, the UAV traveled east at a constant (selectable) velocity and constant (selectable) rate of descent. The trajectory of the intruder was projected from the user-specified closest point of approach at the midpoint of the simulation and projected forward and backward in time based on user-specified flight characteristics.

Two trajectory types were tested for the intruder: a constant-velocity (in all three directions) trajectory and one in which the intruder flew in a circle which varied in altitude. The former was intended to simulate the types of encounters expected along airways while the latter was intended to simulate the limits of expected intruder aircraft maneuvers in controlled airspace. The circular trajectory was drawn such that the intruder aircraft would experience a constant 1G (the force of gravity) centripetal acceleration from level flight for a total of 2Gs force on the aircraft. 2Gs is the force experienced in a 60 degree angle of bank turn in order to maintain level flight. As this is the bank limit for most non-aerobatic aircraft, this was considered the upper limit of what an aircraft could expect to encounter outside of Special Use Airspace (SUA) and aerobatic practice areas.

6.1 Assumptions

Several assumptions were made in conducting the simulations. These are listed below:

- All ADS-B data is accurate as reported (no erroneous or spoofed data).
- TCAS interrogates intruders at 1 Hz.
- Multiple sources of noise can be combined via Root Mean Square (RMS).
- The UAV uses a dual-frequency UAT (no ADS-R used).
- The UAV's UAT has integrated GPS and corrects its clock to UTC time.
- The intruder has a mode-S transponder.
- There are no signal aberrations (e.g.slow fading, fast fading, electromagnetic interference (EMI)).
- Signals propagate at the speed of light in a vacuum.
- The last reported measurement errors of the intruder (from the mode status element) are used in the measurement covariance matrix.
- Measurement errors are uncorrelated with each other.
- The UAV and intruder produce comparably accurate position and velocity estimates.
- The UAV is able to accurately determine its position and velocity at any point in time.
- ADS-B data is appropriately pre-processed (propagation delay is converted to distance and latitude/longitude converted to East and North) with negligible errors.
- Horizontal and vertical speed measurements are comparable in accuracy.

Regarding the last bullet, there are no specifications for the accuracy of reported vertical speed, there is no reported vertical speed accuracy in an ADS-B message, and either geometric

(GPS or Inertial Navigation Systems: INS) or barometric sources may be used to report it. In the absence of other information, the horizontal velocity specifications were used.

Since TCAS and ADS-B data cannot be assumed to arrive at the same time, the ADS-B data is assumed to be projected forward to the time of arrival of the next TCAS return. The possible error induced by this projection is assumed to be zero-mean, Gaussian and is incorporated into the process covariance matrix as described in section 6.2.

6.2 Noise Values

Noise values were selected from data presented in various RTCA documents. A summary of these values can be found in table 6.1.

Measurement Noise Sources		
Component	Source	Range
ADS-B Range	GPS signal in space	$\pm$100 ns
	TX/RX time accuracy	$\pm$500 ns
TCAS Range	TX/RX time accuracy	$\pm$50 ft*
ADS-B Position	Specifications	$\pm$30 m
	Projection	$\pm$2.45 m
ADS-B Velocity	Specifications	$\pm$ 1 m/s
	Projection	$\pm$4.9 m/s
ADS-B Altitude	Specifications	$\leq$ 125 ft
	Projection	$\pm$2.45 m
ADS-B Vertical Speed	Specifications	None (used $\pm$1 m/s)
	Projection	$\pm$4.9 m/s
*Treated as 1σ		

Table 6.1: Measurement Noise Sources and Values

The values in table 6.1 were assumed to be 0.95 (approximately 2σ) values except for the TCAS range noise. This was treated in DO-282B as a 1σ value and was treated as such for simulations.

The ADS-B range noise was derived from the RTCA DO-282B which outlines the worst-case time offset between transmitter and receiver. These values were applied to both aircraft [1].

The TCAS range noise was derived from RTCA DO-300A which specifies that TCAS must not measure the range to intruders with more than 125 ft bias and 50 ft of jitter. These numbers are for mode-S equipped intruders. However, as they are the only TCAS-only range error values specified in DO-300A, they were used for this simulation [2].

ADS-B position, velocity, altitude, and vertical speed specified noise values were applied to both aircraft. The projection noise was only applied to the intruder aircraft.

Measurement Bias Sources		
Component	Source	Range
ADS-B	GPS cable delay	$\leq$ +66 ns
	GPS-UTC time offset	$\pm$1000 ns
	GPS-UAT interconnect delay	$\leq$800 ns
	UAT cable delay	$\leq$ +66 ns
TCAS	Processing delays	$\leq$ +125 ft

Table 6.2: Measurement Bias Sources

Table 6.2 shows the sources of ADS-B and TCAS signal biases specified in DO-282B and DO-300A, respectively. As it was assumed that the UAV utilized a UAT with internal GPS and was synchronized to UTC, neither the GPS-UTC offset nor the GPS-UAT interconnect delay were applied to the UAV. The cable delays, however, were applied to both the UAV and the intruder.

Uniform ADS-B Measurement Errors from LSBs		
Measurement	LSB Value	Range Used
Horizontal Position	2.145672e-5	$\pm$ 1.19 m
Horizontal Velocity	1 kt	$\pm$ 0.26 m/s
Altitude	25 ft	$\pm$ 7.62 m
Vertical Speed	64 ft/min	$\pm$ 0.16 m/s

Table 6.3: Simulated Noise and Bias Values

Table 6.3 shows the errors caused by the transmitting aircraft truncating values to fit the number of bits permitted by the ADS-B message. There is no indication that these errors are accounted for in the mode status element's associated accuracy values. For this reason, they were modeled as normally distributed noise with the upper and lower bounds as specified in table 6.3 [1].

The errors in tables 6.1 and 6.3 were combined via RMS to produce the diagonal terms used in the measurement covariance matrix. Although the errors caused by LSB truncation are uniformly distributed, this method of treating them like normally-distributed 2σ values was used in DO-300A so was considered sufficiently representative [2].

The continuous process variances used for the simulations are shown in table 6.4. These values were only starting points and adjusted after the initial tests were conducted to improve performance.

Continuous Process Covariance Values	
Component	Value
$N_{\dot{s}}$	1.3 $(m/s)^2/s$
$N_{\ddot{s}}$	0.3 $(m/s^2)^2/s$

Table 6.4: Continuous Process Covariance Values

6.3 Test Cases

To validate each model discussed above, simulations were run using perfect measurements (simulated measurements with no noise). All models provided perfect state estimates when provided perfect measurements. To test the robustness of the models, several scenarios were examined. These scenarios are summarized below:

- Baseline: noisy measurements with both TCAS and ADS-B ranges with no measurement loss
- ADS-B as the only range measurement
- TCAS as the only range measurement
- No range measurements
- 15% random measurement loss
- 10 second signal outages

Parameters used for the tests are outlined in table 6.5. The high speed was chosen to be representative of large aircraft at high altitudes. For linear trajectories, the intruder aircraft flew at 90 degree angles to the UAV so horizontal position errors caused by velocity uncertainty were consistent in both directions. The rates of descent are consistent with what is expected on airways and the point of closest approach was chosen to be zero for all directions to detect any aberrations in estimates as the separation dropped to zero.

Simulation Parameters	
Component	Value
UAV Speed	500 kts
Intruder Speed	500 kts
Closest Point of Approach	0 E, 0 N, 0 U
Intruder Vertical Speed	1000 ft/min
UAV Vertical Speed	-1000 ft/min
UAV heading	090
Intruder heading (linear)	180

Table 6.5: Test Parameters

The above scenarios were tested for both a linear and a circular trajectory. The results of these tests are compiled in chapter 7.

Chapter 7

Results

Graphical results from the test cases described above are shown below with detailed statistics contained in the appendix.

7.1 Baseline

Baseline results showed improved position, velocity, and (when applicable) acceleration estimates over unprocessed ADS-B data. The EKF with no delay states slightly outperformed the others when the intruder flew the linear trajectory.

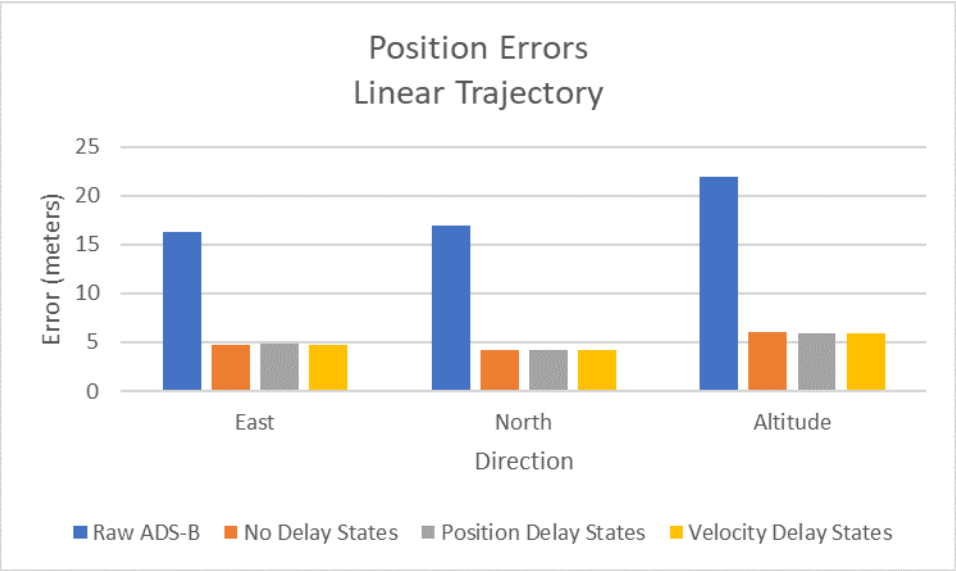

Figure 7.1: Average Position Errors for Various Models

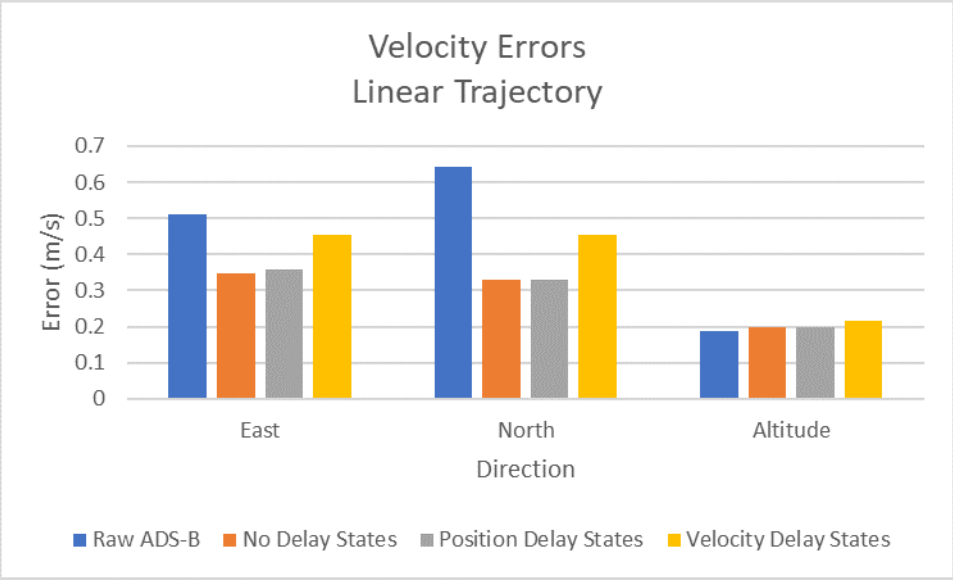

Figure 7.2: Average Velocity Errors for Various Models

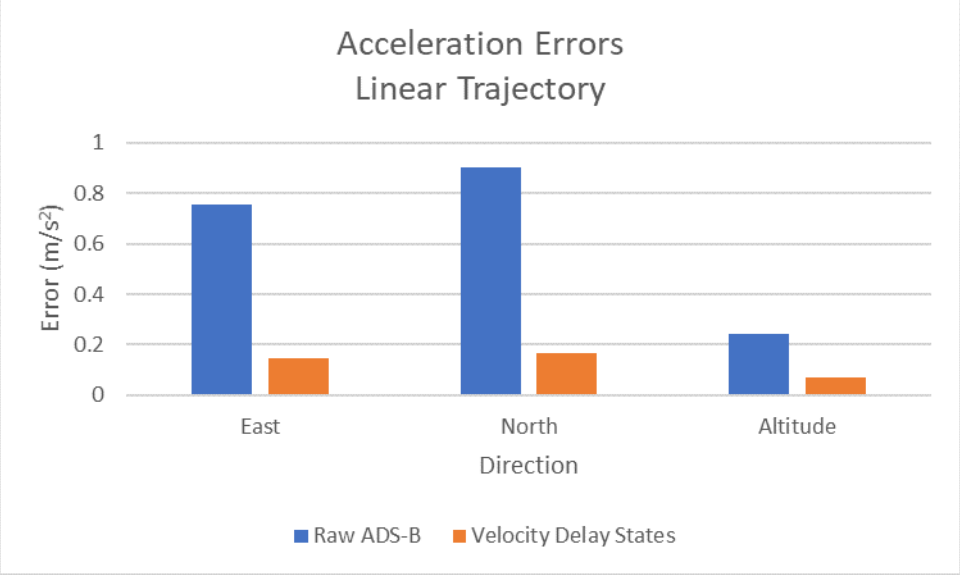

Figure 7.3: Average Acceleration Errors for Various Models

The EKF with velocity delay states out performed the other two when the intruder flew a circular trajectory. Both the other EKFs yielded large velocity errors when using the process noise values previously described.

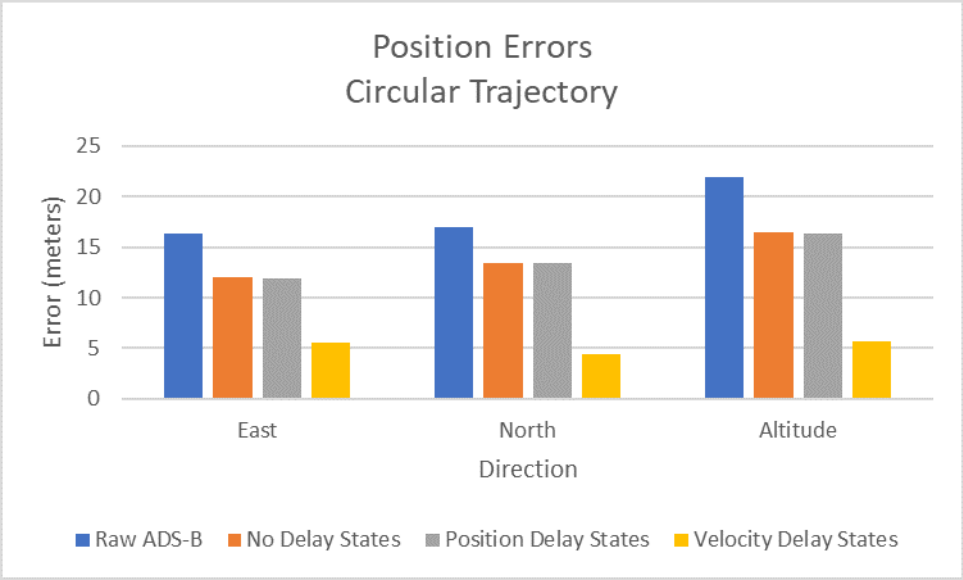

Figure 7.4: Average Position Errors for Various Models

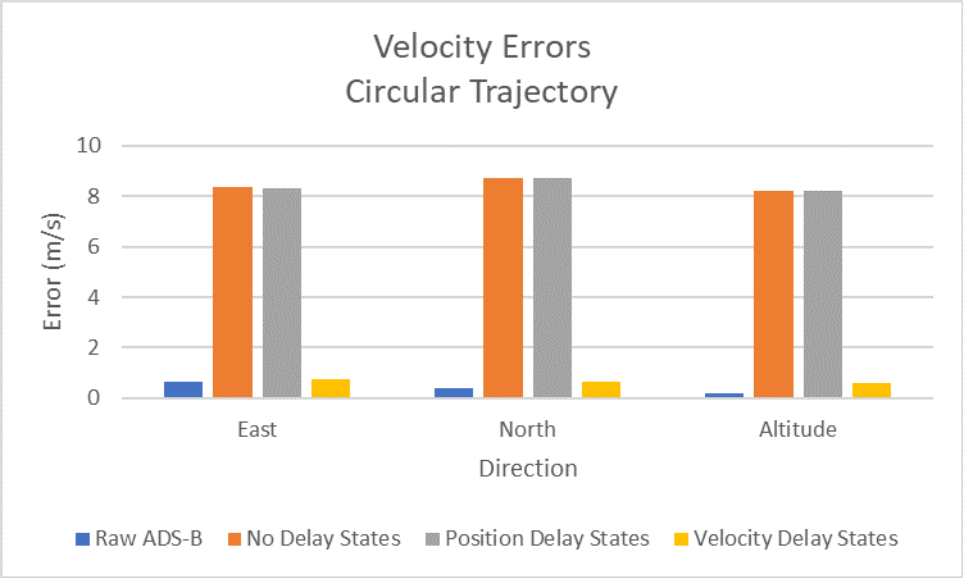

Figure 7.5: Average Velocity Errors for Various Models

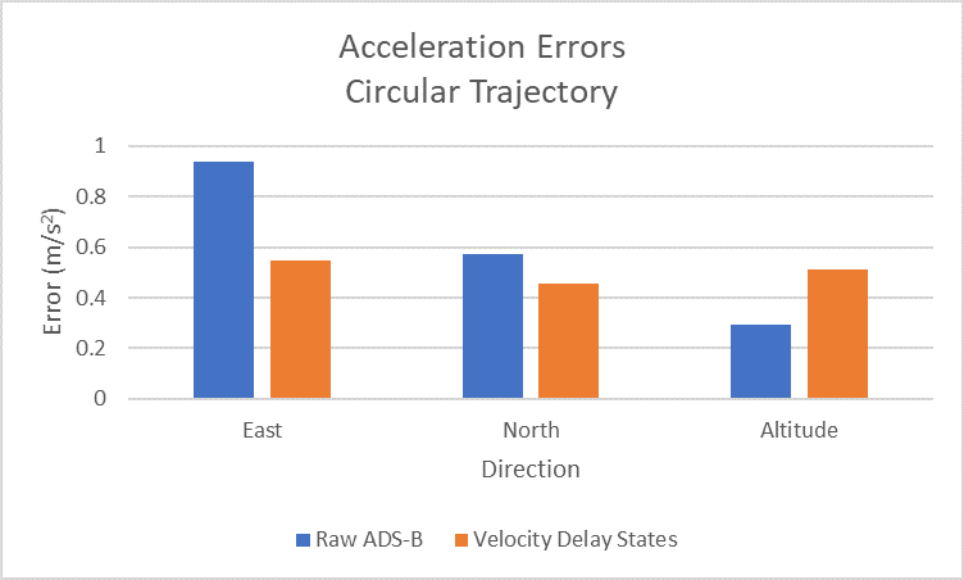

Figure 7.6: Average Acceleration Errors for Various Models

7.2 TCAS Range Only

When the only range measurement used was from TCAS, all three EKFs outperformed ADS-B unprocessed data with the EKF sans delay states showing slightly better results than the other two when the intruder flew a linear trajectory.

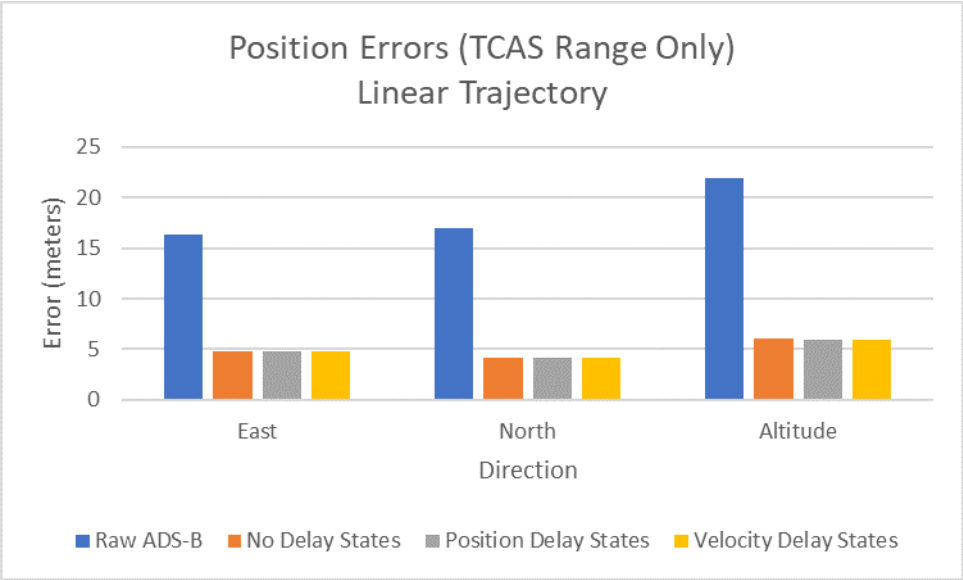

Figure 7.7: Average Position Errors for Various Models with Only TCAS Range

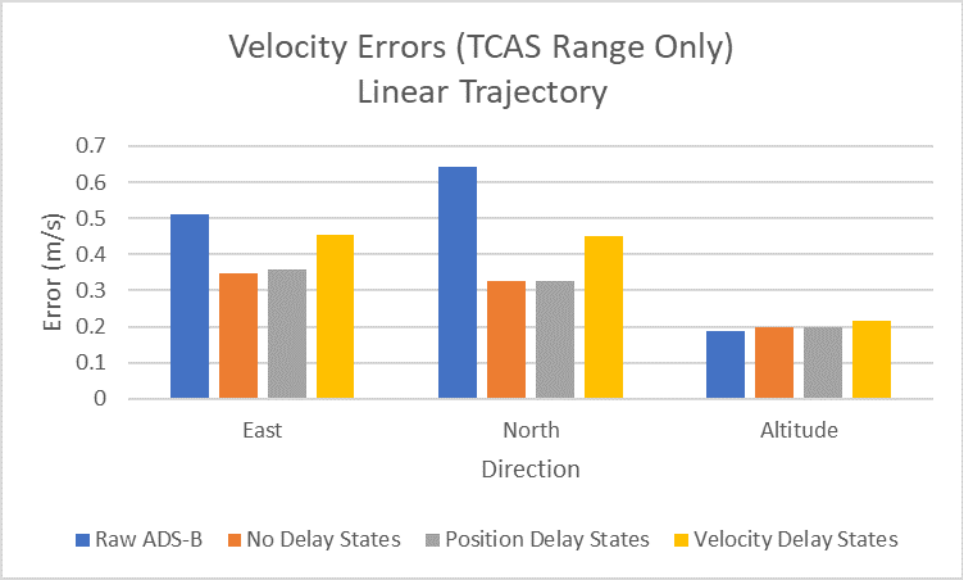

Figure 7.8: Average Velocity Errors for Various Models with Only TCAS Range

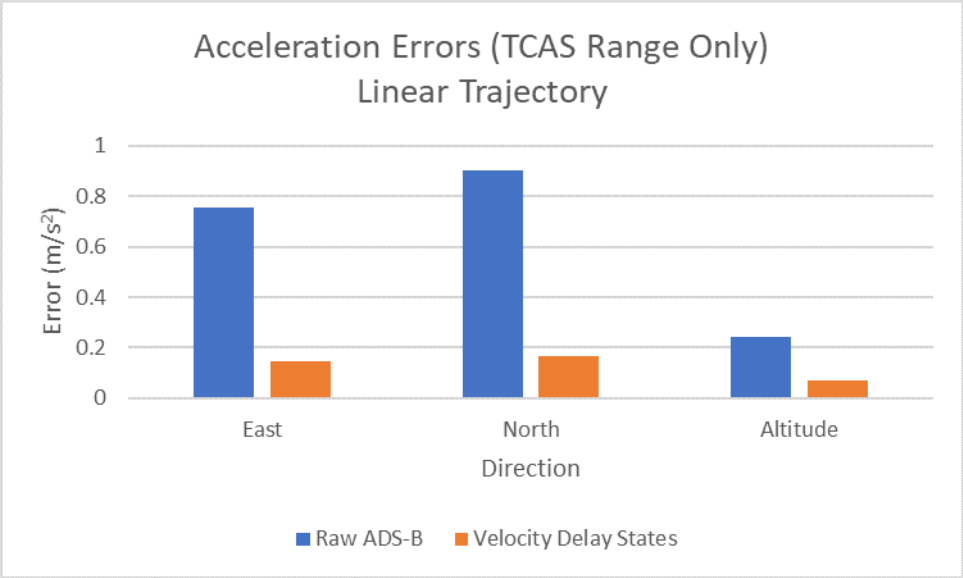

Figure 7.9: Average Acceleration Errors for Various Models with Only TCAS Range

When the intruder flew a circular trajectory, the EKF with velocity delay states provided the best results.

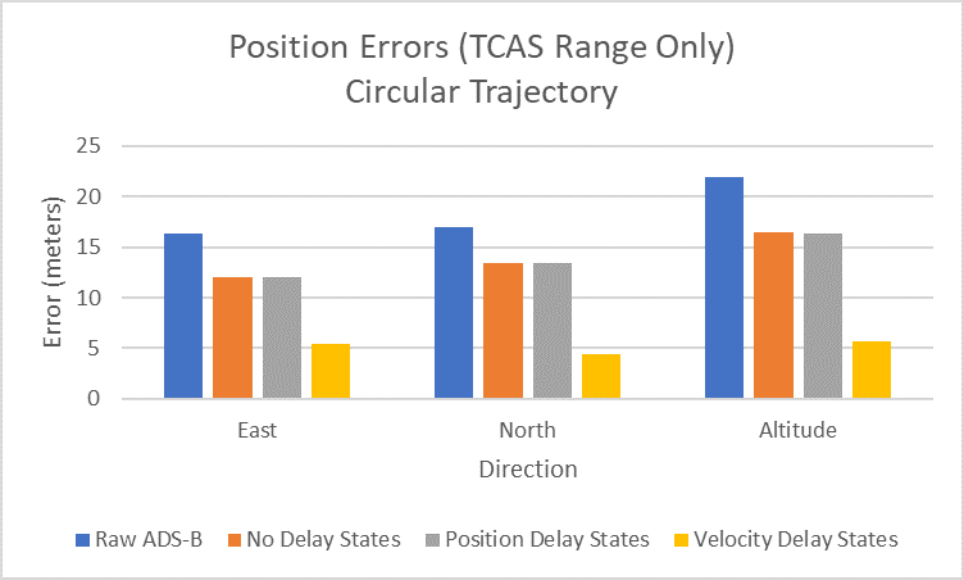

Figure 7.10: Average Position Errors for Various Models with Only TCAS Range

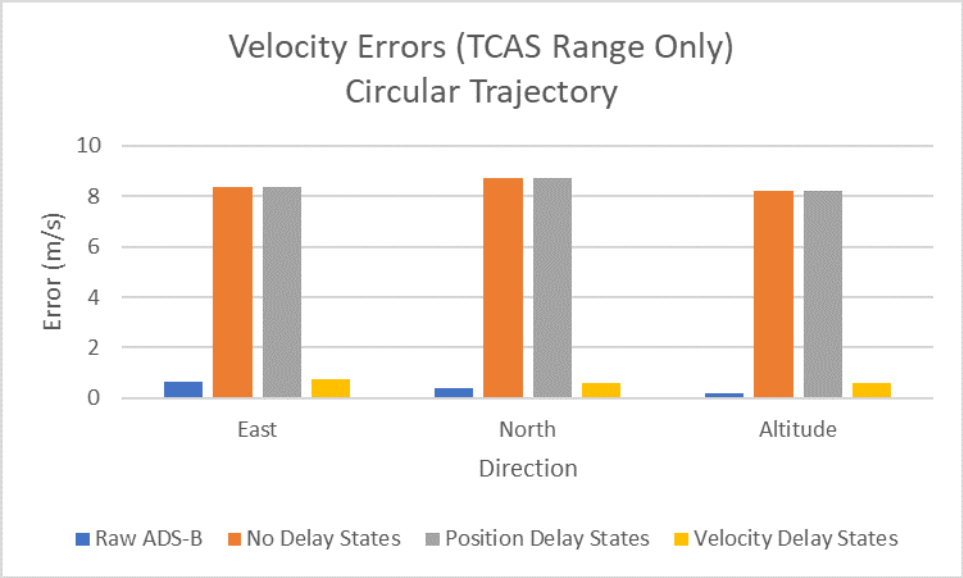

Figure 7.11: Average Velocity Errors for Various Models with Only TCAS Range

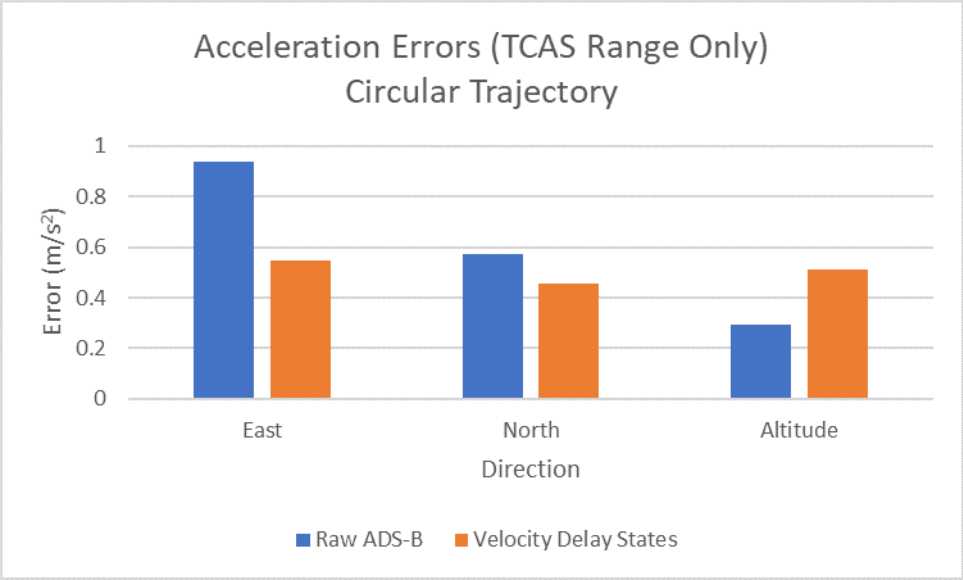

Figure 7.12: Average Acceleration Errors for Various Models with Only TCAS Range

7.3 ADS-B Range Only

As the ADS-B range measurement is noisier, the EKFs were less accurate when only utilizing it for range measurement. Again, the EKF without delay states was the best filter by a small margin.

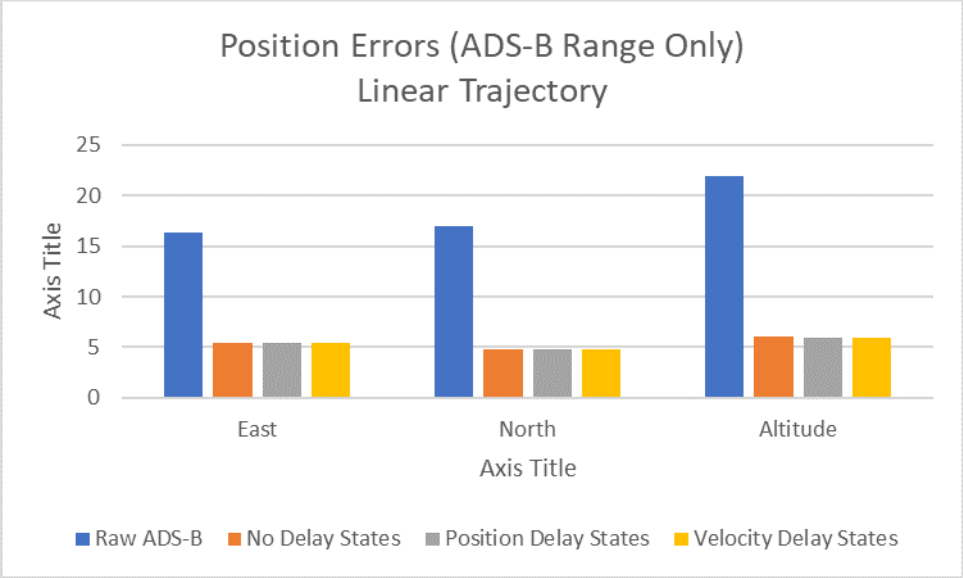

Figure 7.13: Average Position Errors for Various Models with Only ADS-B Range

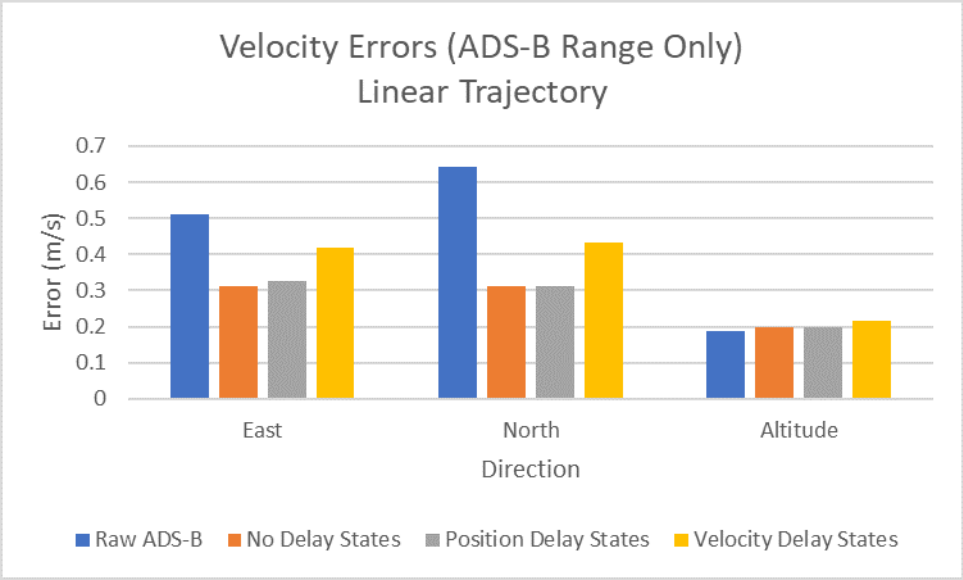

Figure 7.14: Average Velocity Errors for Various Models with Only ADS-B Range

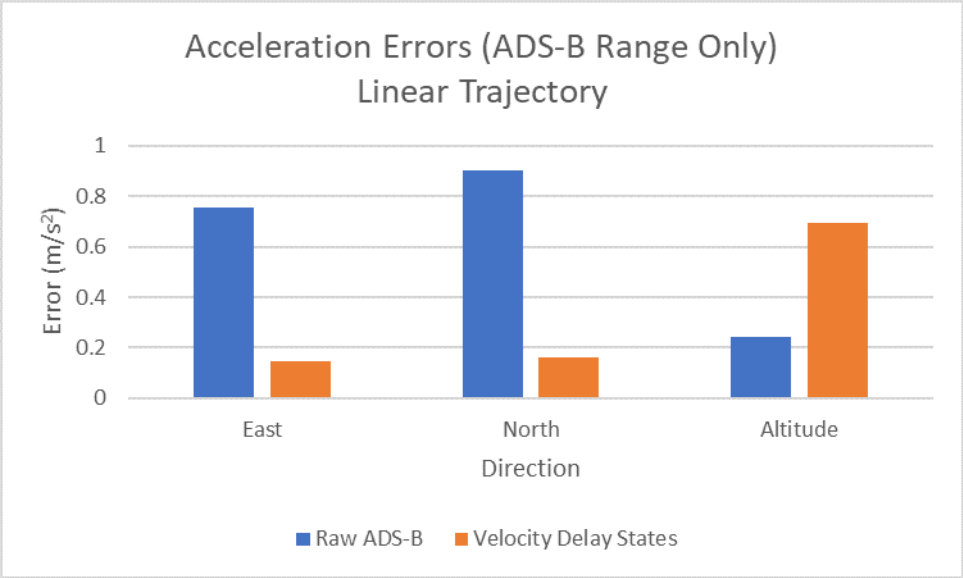

Figure 7.15: Average Acceleration Errors for Various Models with Only ADS-B Range

The EKF using velocity delay states outperformed the other two when the intruder's trajectory was circular.

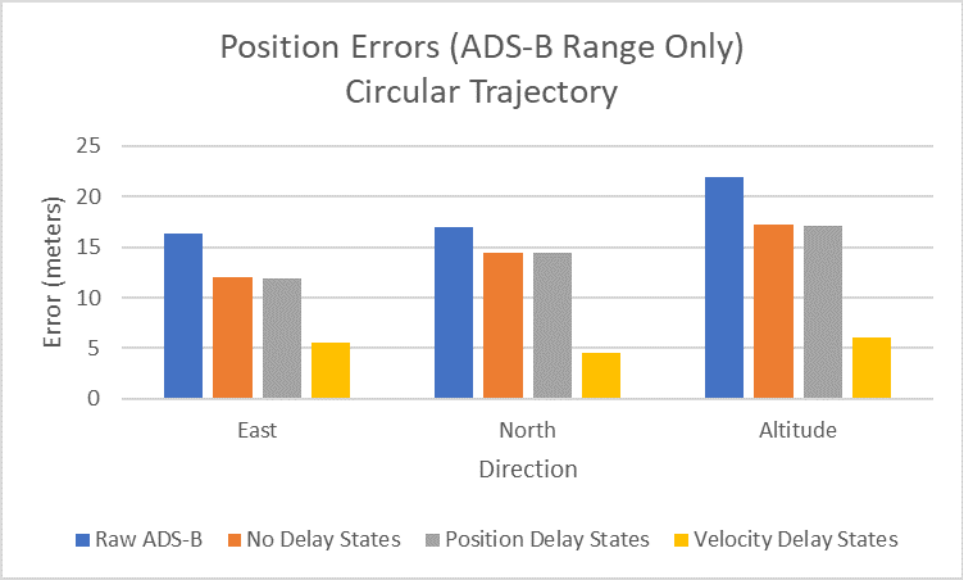

Figure 7.16: Average Position Errors for Various Models with Only ADS-B Range

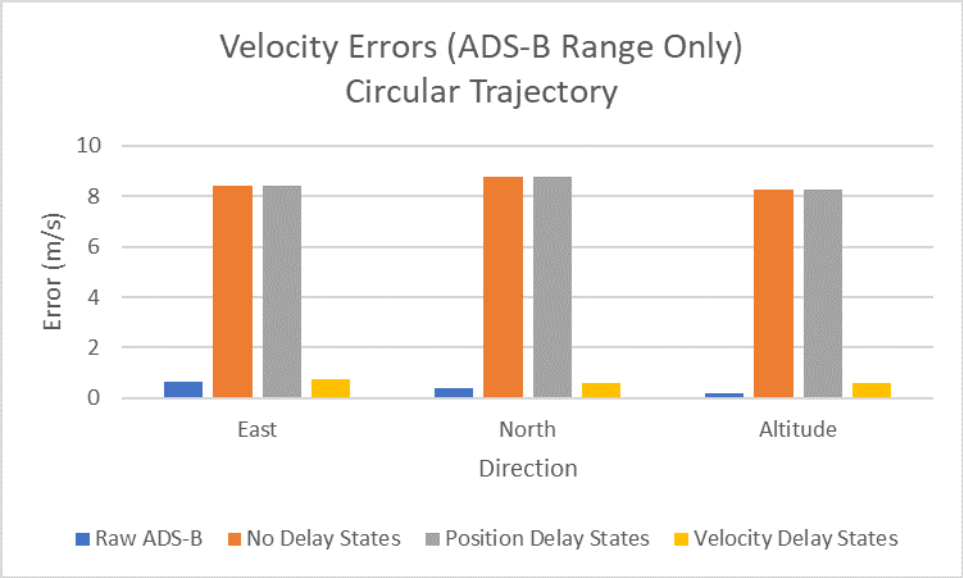

Figure 7.17: Average Velocity Errors for Various Models with Only ADS-B Range

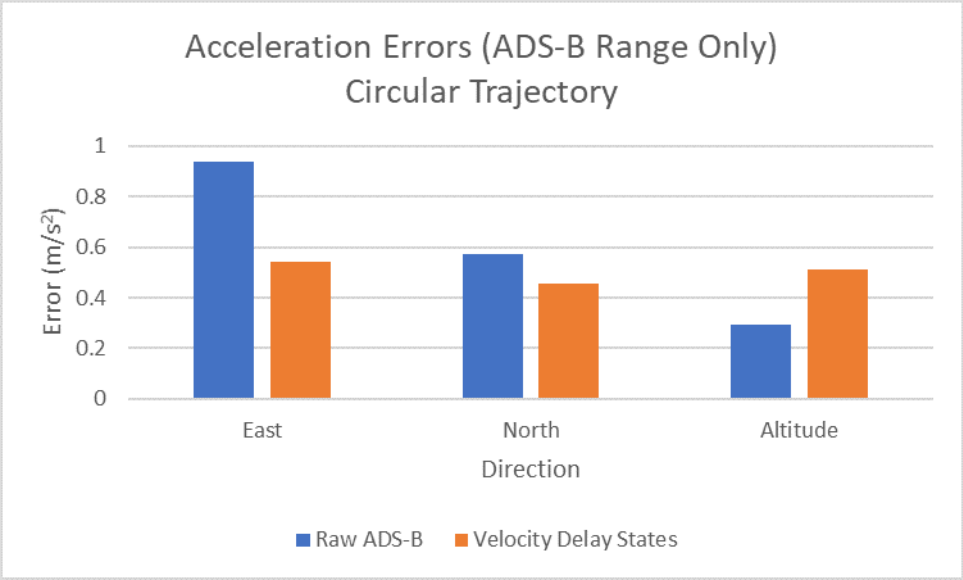

Figure 7.18: Average Acceleration Errors for Various Models with Only ADS-B Range

7.4 No Range Measurements

Surprisingly, the EKFs produced slightly more accurate position and velocity estimates when no range measurements were used than when only ADS-B range was used. The EKF with no delay states slightly out-performed the other two when the intruder flew a linear trajectory.

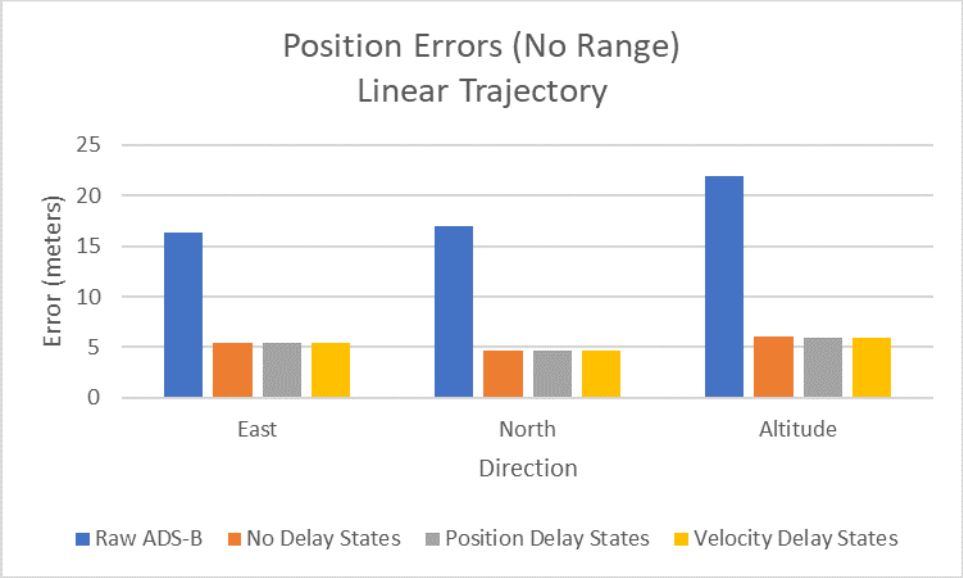

Figure 7.19: Average Position Errors for Various Models with No Ranges

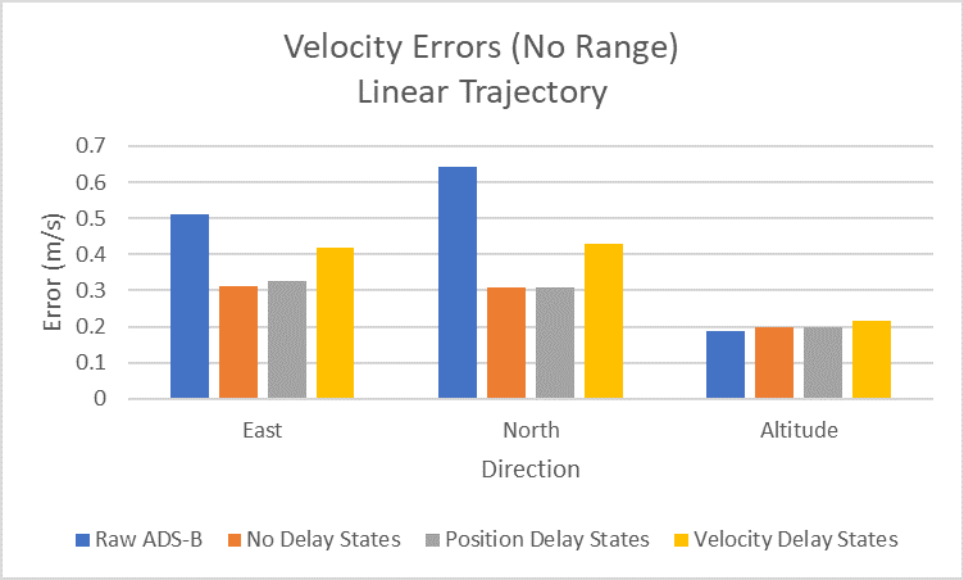

Figure 7.20: Average Velocity Errors for Various Models with No Ranges

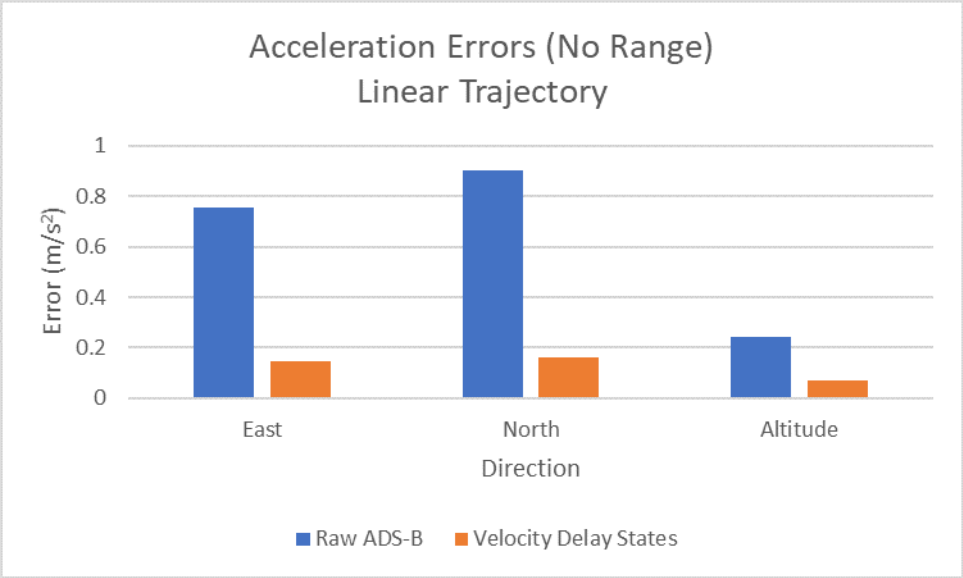

Figure 7.21: Average Acceleration Errors for Various Models with No Ranges

When the intruder's trajectory was circular, the EKF with velocity delay states produced the best results of the three.

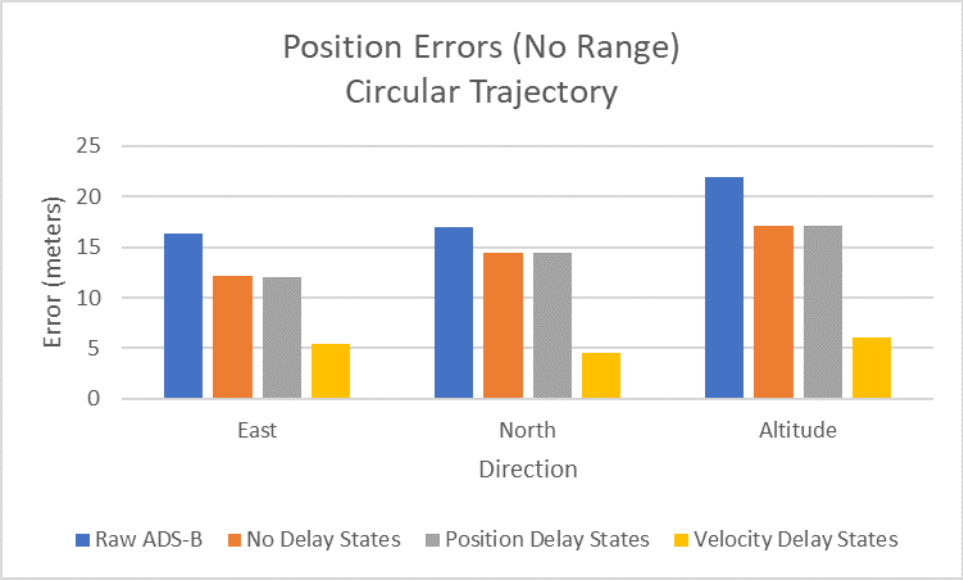

Figure 7.22: Average Position Errors for Various Models with No Ranges

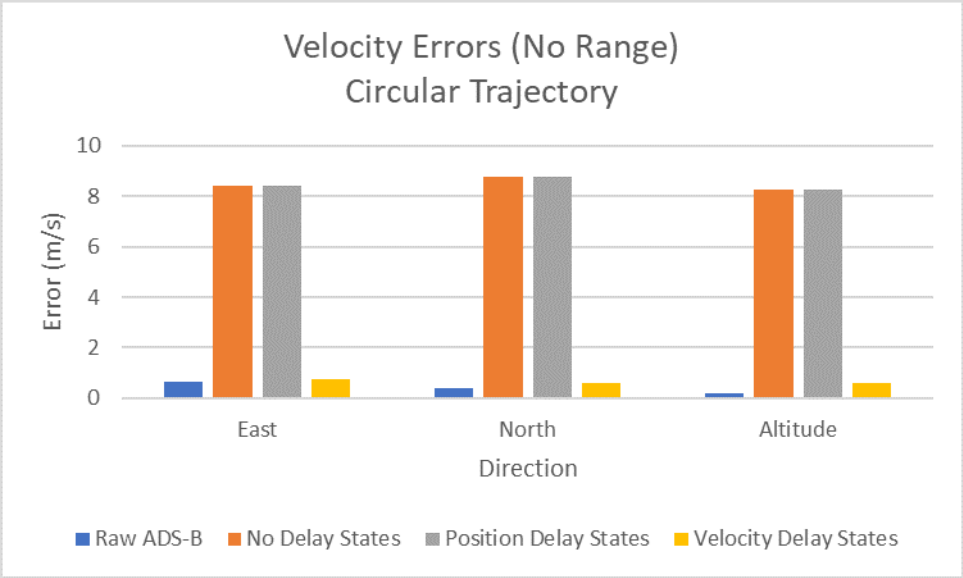

Figure 7.23: Average Velocity Errors for Various Models with No Ranges

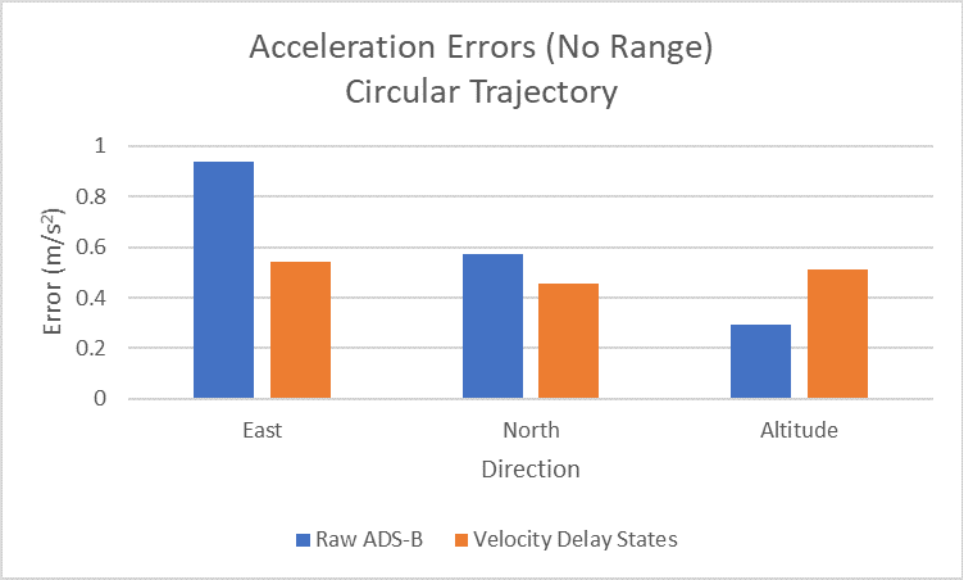

Figure 7.24: Average Acceleration Errors for Various Models with No Ranges

7.5 15% Measurement Loss

When 15% of the measurements were randomly lost, the accuracy of all three filters degraded somewhat. The EKF with with velocity delay states, however, performed very poorly; ADS-B unprocessed measurements were more accurate for both the intruder's linear and circular trajectories.

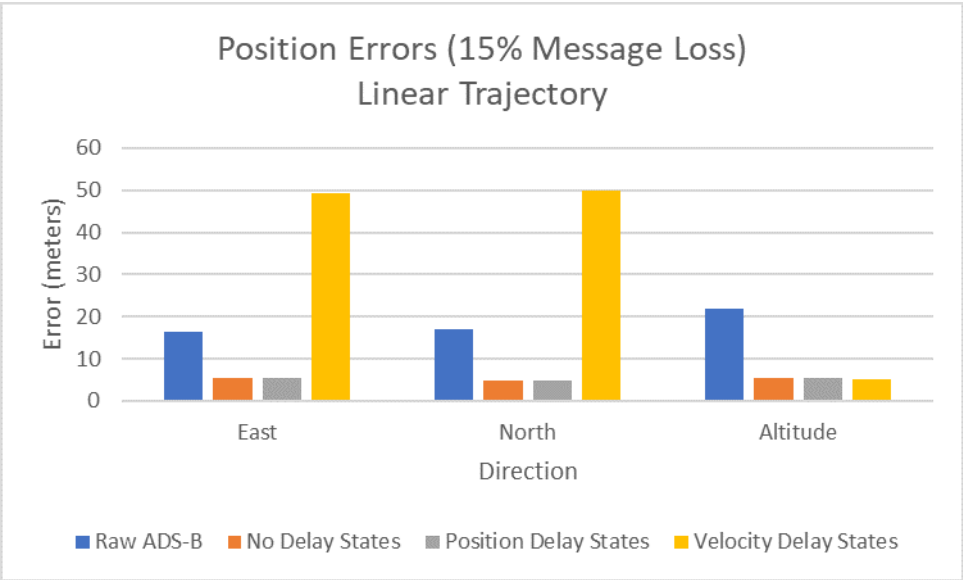

Figure 7.25: Average Position Errors for Various Models with 15% Message Loss

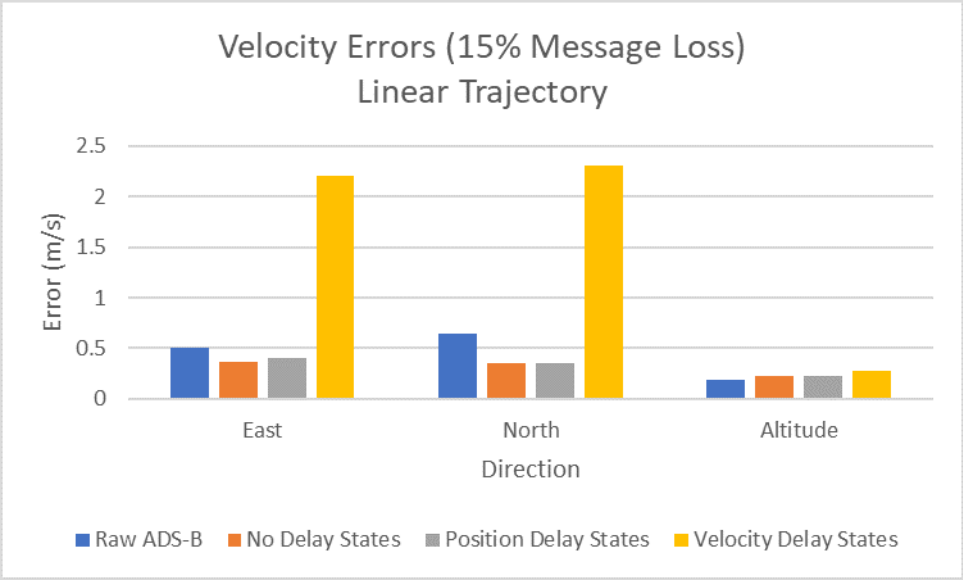

Figure 7.26: Average Velocity Errors for Various Models with 15% Message Loss

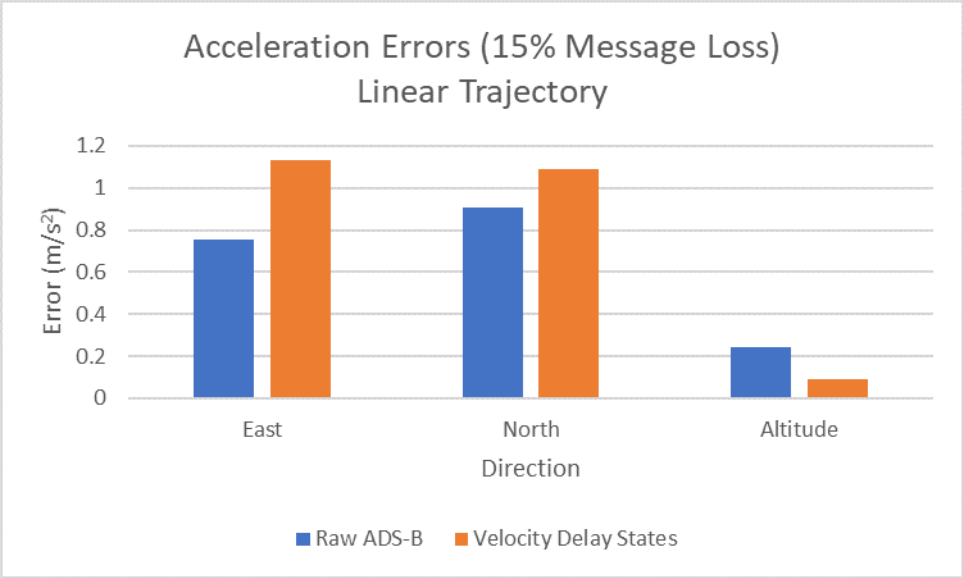

Figure 7.27: Average Acceleration Errors for Various Models with 15% Message Loss

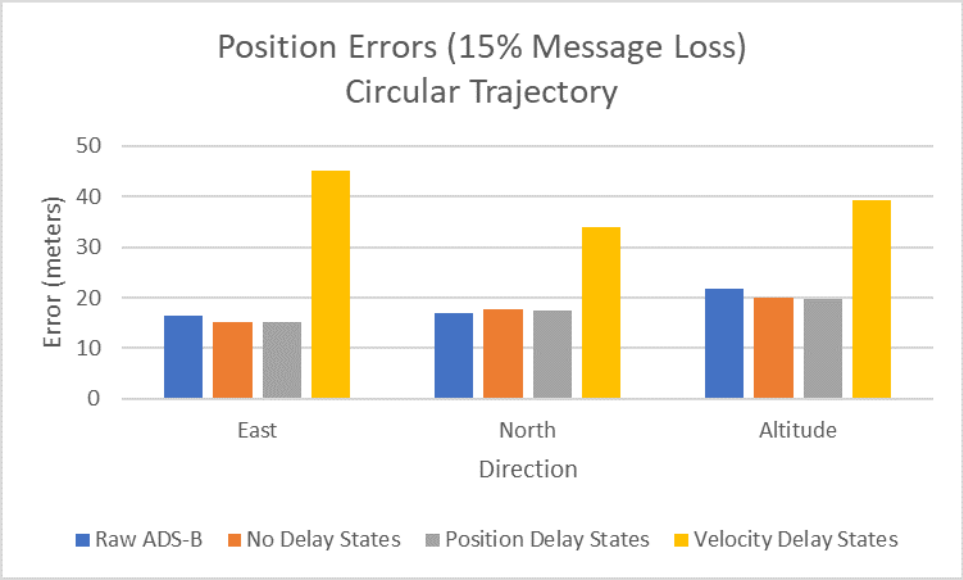

Figure 7.28: Average Position Errors for Various Models with 15% Message Loss

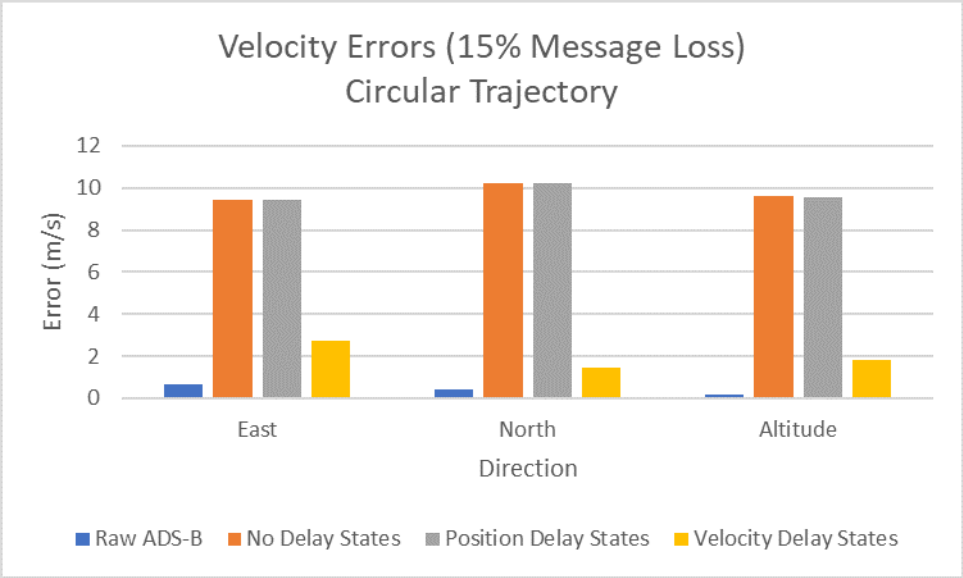

Figure 7.29: Average Velocity Errors for Various Models with 15% Message Loss

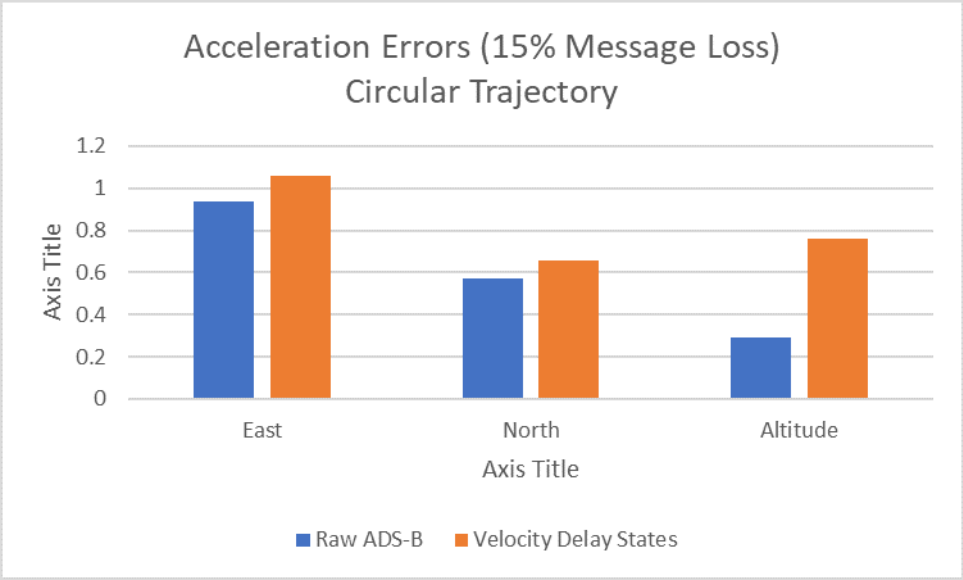

Figure 7.30: Average Acceleration Errors for Various Models with 15% Message Loss

Attempts were made to improve the performance of the EKF with velocity delay states by adjusting the process noise values. No value could be found which brought the average error to less than that of unprocessed ADS-B data when 15% of the measurements were missing.

7.6 Tuning the EKF with No Delay States

As the EKF with velocity delay states performed so poorly when measurements were lost and the other two filters were of comparable accuracy under all of the tests conducted above, the EKF with no delay states was selected as the most promising and explored further. The continuous process noise parameters were adjusted to see if improvements could be made to the results when the intruder flew a circular trajectory. The following figures show the error trends for various process noise values.

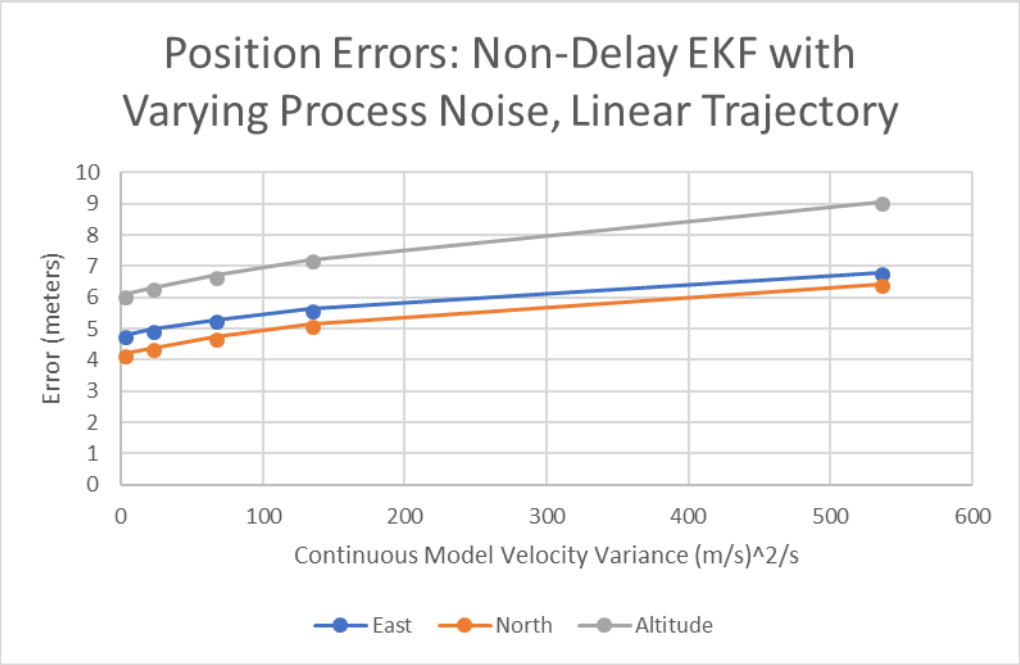

Figure 7.31: Average Position Errors for Various Process Noise Values

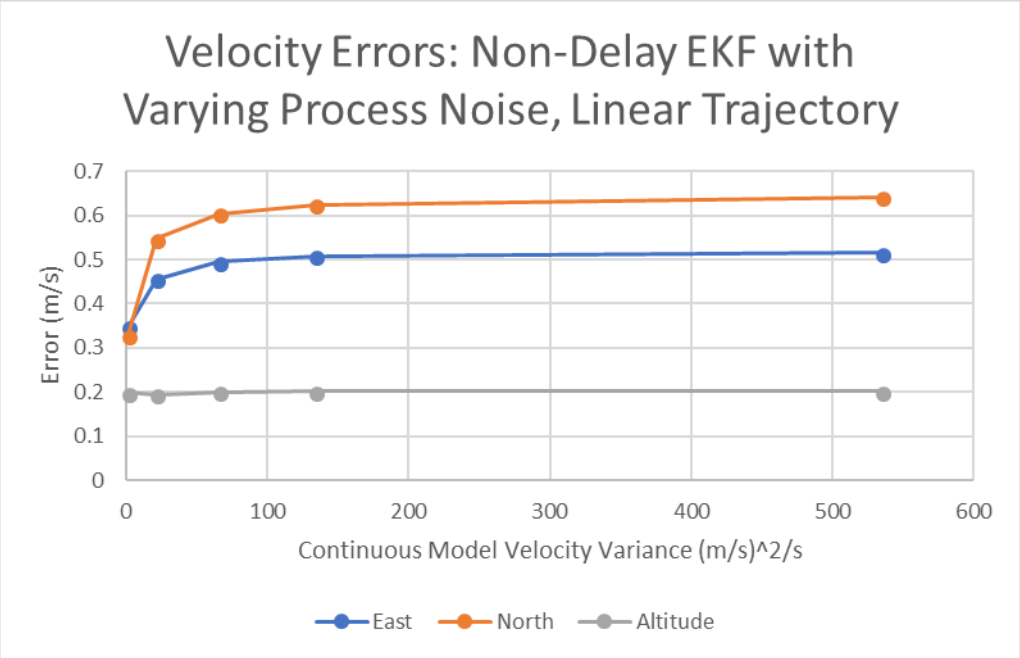

Figure 7.32: Average Velocity Errors for Various Process Noise Values

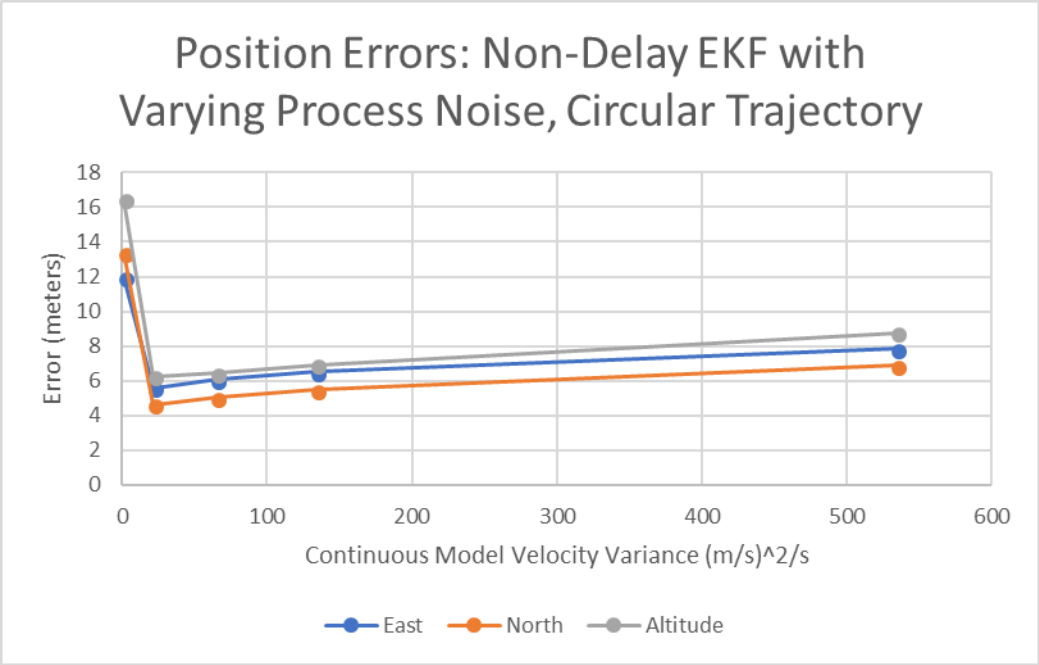

Figure 7.33: Average Position Errors for Various Process Noise Values

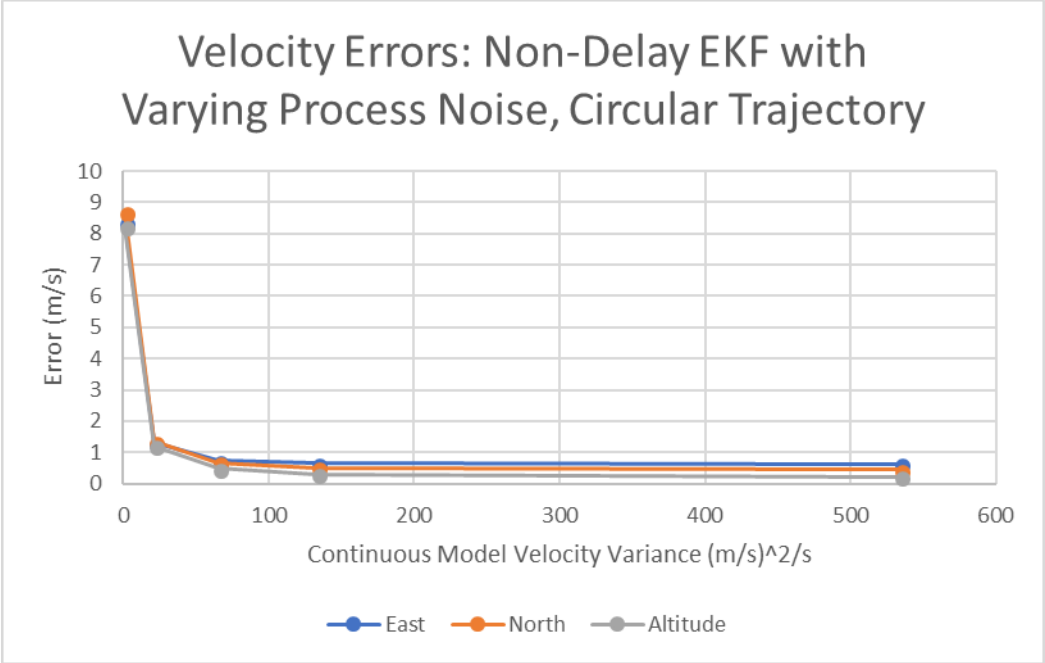

Figure 7.34: Average Velocity Errors for Various Process Noise Values

There was a dramatic decrease in the position and velocity errors for an intruder flying a circular trajectory when the process noise was increased. There was a corresponding slight increase in velocity error for the intruder's linear path. Given the results above, 65 $(m/s)^2/s$

was selected as the best continuous process noise variance. Further resolution was considered unwarranted for simulated data.

7.7 Evaluating Range Measurement Contributions

To determine the contribution of TCAS and ADS-B range measurements toward resolving the relative position and velocity between the UAV and the intruder, simulations with and without the ranges were conducted. The results are shown below:

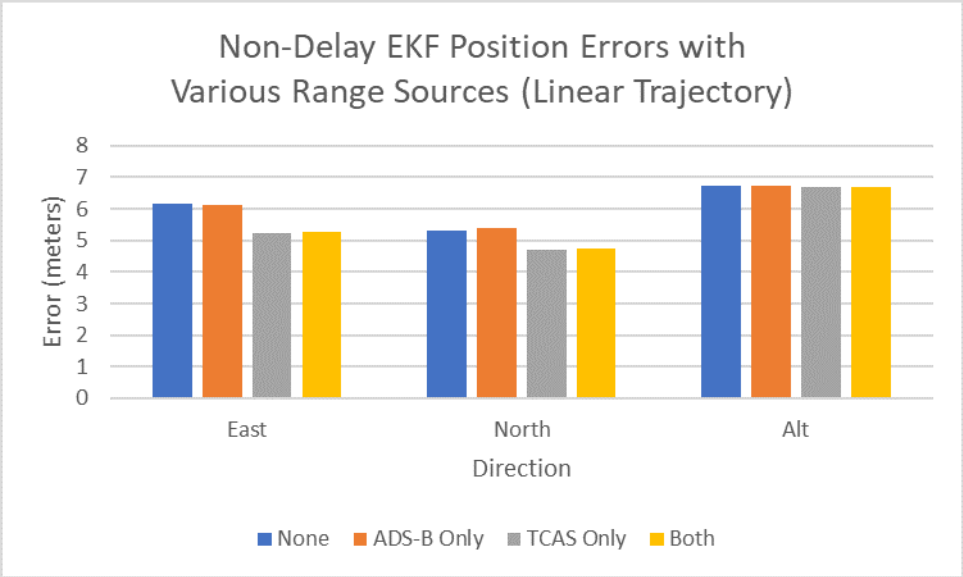

Figure 7.35: Average Position Errors for Various Range Measurements

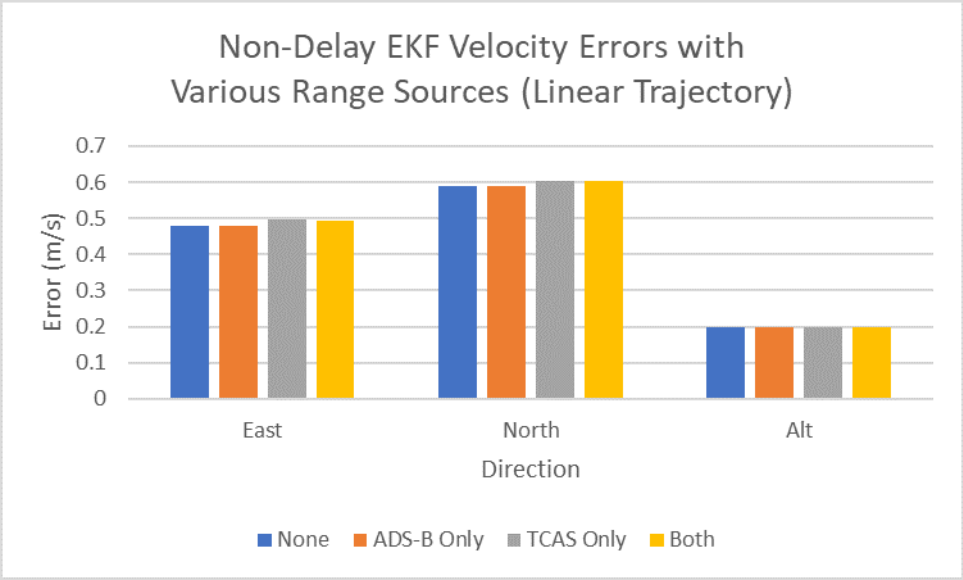

Figure 7.36: Average Velocity Errors for Various Range Measurements

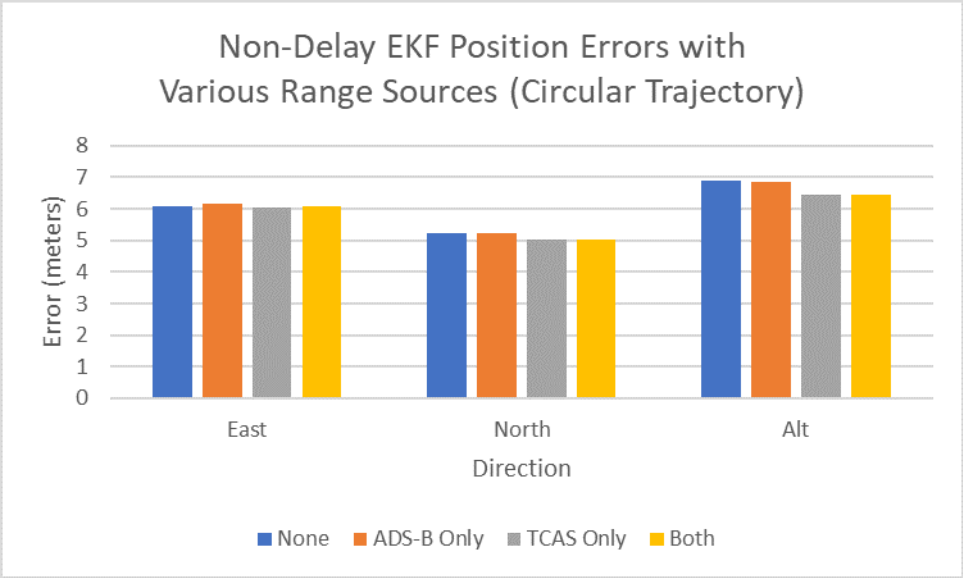

Figure 7.37: Average Position Errors for Various Range Measurements

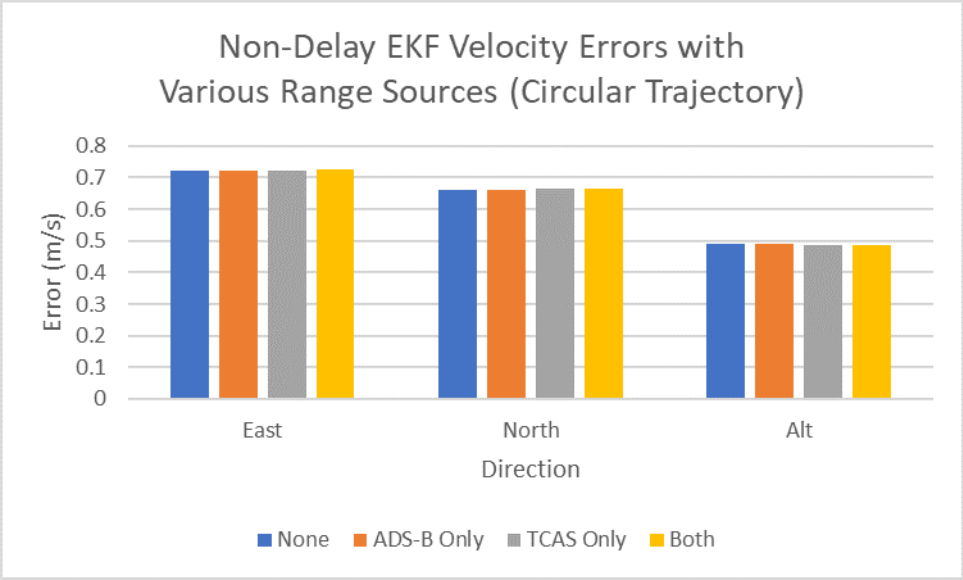

Figure 7.38: Average Velocity Errors for Various Range Measurements

TCAS range measurements without ADS-B range measurements offered the best improvement in position errors. The inclusion of range measurements slightly increased the error in relative velocity estimates. Since TCAS range measurements offered the best position estimate improvement with only a small cost to velocity estimates, the EKF was validated using TCAS range measurements.

7.8 Validating the EKF with No Delay States

The following figures show the tuned EKF outperformed ADS-B unprocessed position estimates for both the intruder's linear and circular trajectories. The filter offered improvement over ADS-B reported velocity for the linear trajectory when no measurements were missing, but not for the circular trajectory nor when 15% of the measurements were missing.

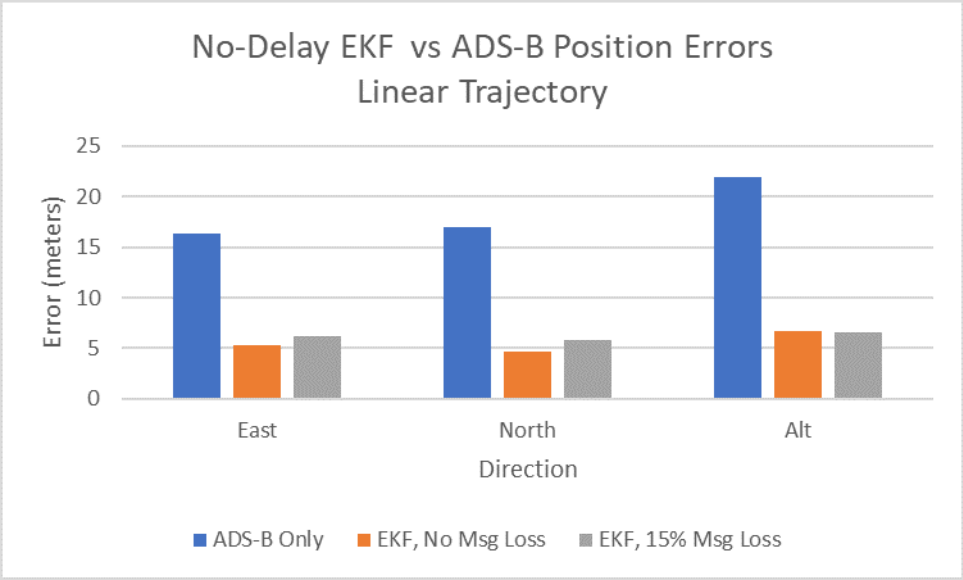

Figure 7.39: Average Position Errors for No Delay EKF vs ADS-B Only

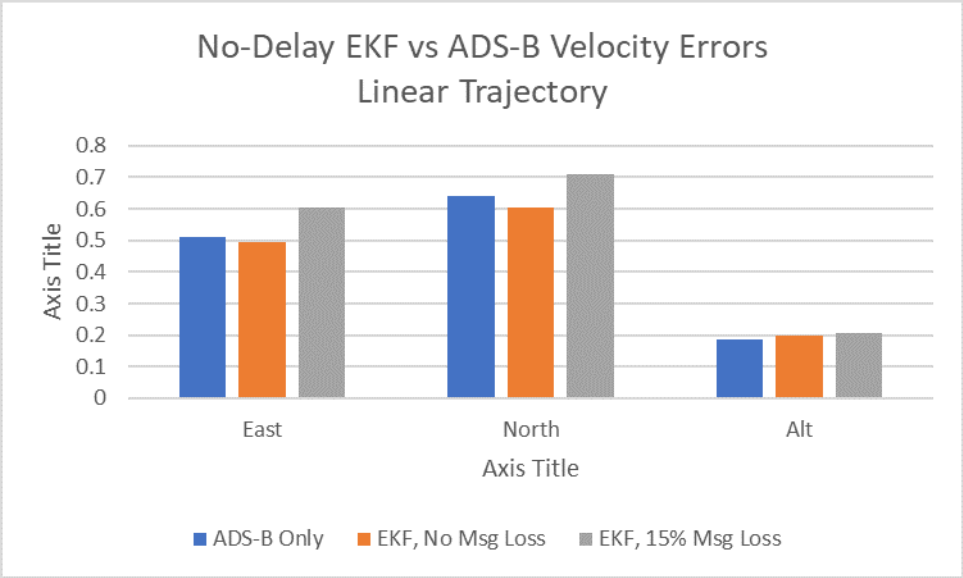

Figure 7.40: Average Velocity Errors for No Delay EKF vs ADS-B Only

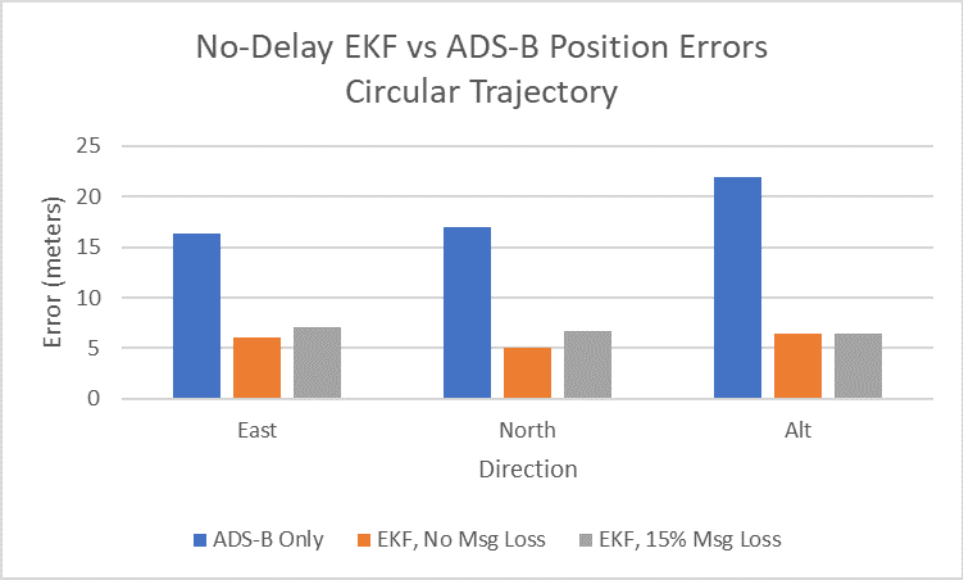

Figure 7.41: Average Position Errors for No Delay EKF vs ADS-B Only

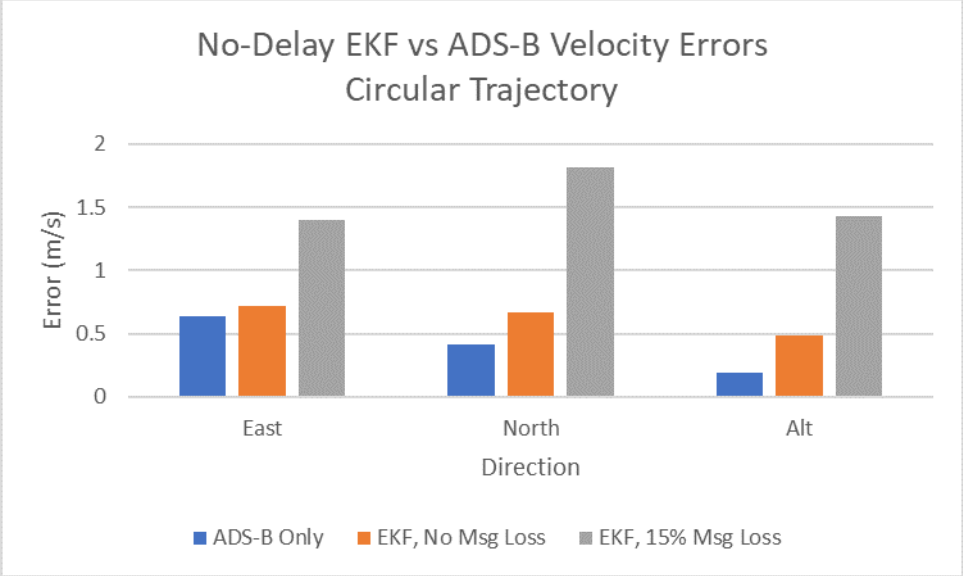

Figure 7.42: Average Velocity Errors for No Delay EKF vs ADS-B Only

The EKF was also tested with a 10 second signal outage. This outage is intended to represent a momentary shielding of the transmitting antenna when the UAV or intruder is in an attitude or relative position such that part of either aircraft obscures the antenna (e.g. the wing during a turn). Plots of the errors and error envelopes for the linear trajectory are shown below. The circular trajectory is omitted since the errors will vary depending on the timing of the signal loss.

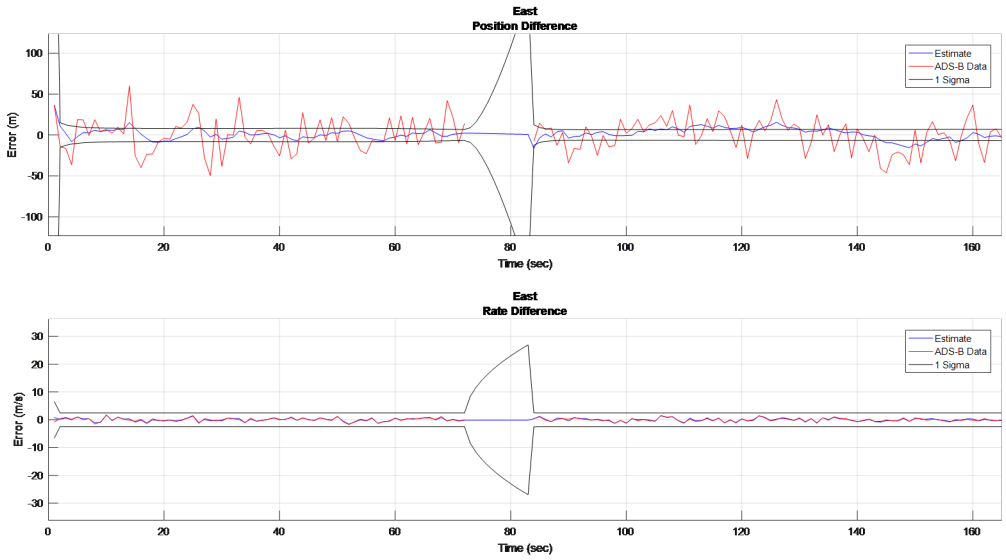

Figure 7.43: East Position and Velocity Errors with Error Envelope for 10 Second Signal Outage (Linear Trajectory)

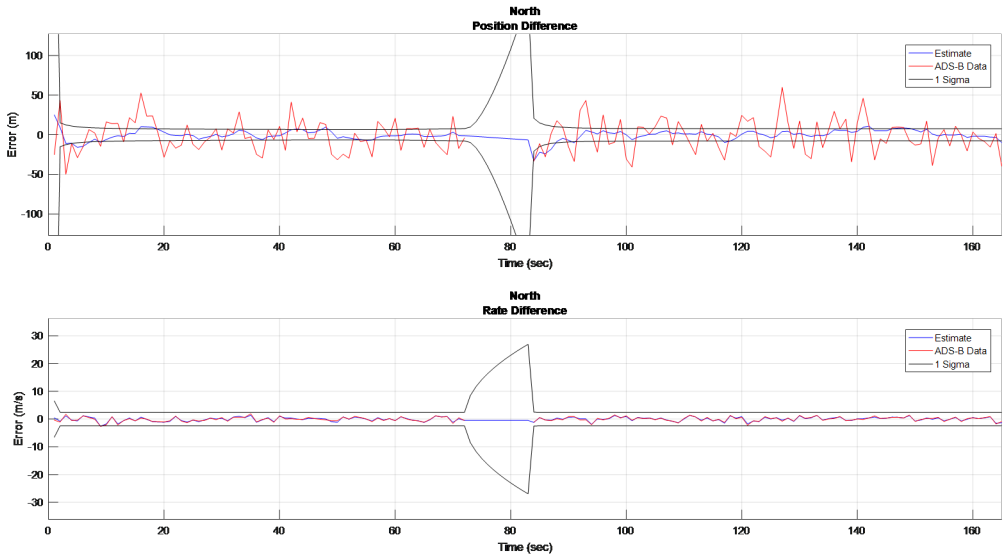

Figure 7.44: North Position and Velocity Errors with Error Envelope for 10 Second Signal Outage (Linear Trajectory)

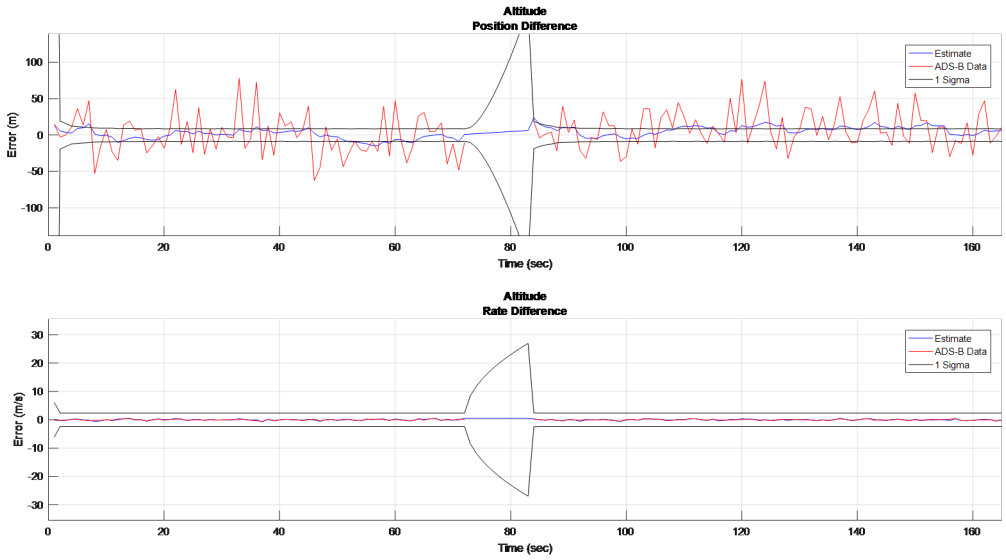

Figure 7.45: Altitude and Vertical Speed Errors with Error Envelope for 10 Second Signal Outage (Linear Trajectory)

Chapter 8

Conclusions

The EKF with no delay states was the best optimal estimator tested. Although the EKF with velocity delay states performed very well in the presence of measurements, its poor performance with 15% measurement loss precluded it from being considered. The EKF with no delay states was also easy to tune and when it was tuned, provided good performance under all circumstances tested. It would be an easy filter to tune when provided actual ADS-B data. Given that the filter provided better estimates of the linear trajectory with low process noise values and better estimates of the circular trajectory with larger process noise values, the best option may be to use a lower process noise value when flying airways (where minimal maneuvering can be expected) and a larger noise value when approaching the terminal environment.

The EKF with no delay states was also the least complex filter tested. With no delay states, the measurement and process noise were uncorrelated and the additional complexity of accounting for such correlation was unnecessary. A lack of delay states also meant there was no need to retain measurement values and matrices from previous time steps nor deal with the issue of how to handle measurements with delay states when one of the two terms was missing.

The slight degradation in EKF performance when including ADS-B range measurements was attributed to the large amount of noise in these measurements. If actual flight data showed typical noise to be less than that assumed here, it may be worth the effort to incorporate the range measurements. As it stands, it appears best to use the ADS-B range only to validate ADS-B reports rather than attempt to augment them.

TCAS range measurements at times offered nearly a meter in improved position accuracy over no range measurements likely due to their low noise levels. It is worth investigating their

incorporation with actual flight data. If ADS-B data consistently provides accurate position and velocity estimates, it may turn out the difficulty associated with incorporating TCAS range is not worth the slight benefit.

Chapter 9

Future Work

The most obvious task to be accomplished in the future is to test the EKFs presented under actual flight conditions. Hardware rarely matches simulated behavior under actual usage conditions. No definitive statement about the utility of the EKFs presented can be made without flight tests.

Should the EKFs provide promising results when used with nominal flight data, the limits of their utility should be tested. The EKFs should be presented with aerobatic aircraft data, spurious data, and extremely noisy data which would not normally permit its use for collision avoidance.

The information provided by UATs has the potential to permit completely autonomous taxi, takeoff, flight, landing, and taxi to parking. As ADS-B messages are transmitted by ground vehicles, modified collision avoidance logic can be used by UAVs on the ground to taxi between parking and the active runway. As discussed in section 2.1.2, ADS-B mode status messages contain a large amount of data which could be used to select the best collision avoidance maneuver. Such data could be considered for use in UAV collision avoidance logic. If/when TC messages are implemented, their data can be used to further refine UAV collision avoidance logic. Finally, the periodic weather and airspace updates provided by UATs could be used in conjunction with collision avoidance logic to provide globally optimal path planning from the moment a UAV taxis from parking at its starting airport to the moment it shuts down at its destination.

References

[1] RTCA Special Committee 186, ”Minimum Operational Performance Standards (MOPS) for Universal Access Transceiver (UAT) Automatic Dependent Surveillance - Broadcast (ADS-B),” RTCA, Inc., 2011.

[2] RTCA Special Committee 147, “Minimum Operational Performance Standards (MOPS) for Traffic Alert and Collision Avoidance System II (TCAS II) Hybrid Surveillance,” RTCA, Inc., 2013.

[3] RTCA Special Committee 186, “Minimum Aviation System Performance Standards (MASPS) for ADS-B Traffic Surveillance Systems and Applications (ATSSA),” RTCA, Inc., 2012.

[4] Federal Aviation Administration, “Title 14 of the Code of Federal Regulations (14 CFR),” Federal Aviation Administration, 2018.

[5] Federal Aviation Administration, “Aeronautics Informaiton Manual (AIM),” Federal Aviation Administration, 2018.

[6] Federal Aviation Administration, “Introduction to TCAS II Version 7.1,” Federal Aviation Administration, 2011.

[7] Balaji Raman Katta and Irfan Madani, “Traffic avoidance and separation system,” 2017 International Conference on Advances in Computing, Communications and Informatics (ICACCI), 2017.

[8] Subramanian Ramasamy and Roberto Sabatini, “A Unified Approach to Cooperative and Non-Cooperative Sense-and-Avoid ,” 2015 International Conference on Unmanned Aircraft Systems (ICUAS), 2015.

[9] Chizhao Yang, Jared Strader, Yu Gu, and Alexander Hypes, “Cooperative UAV Navigation using Inter-Vehicle Ranging and Magnetic Anomaly Measurements,” 2018 AIAA Guidance, Navigation, and Control Conference, 2018.

[10] Brown, G.R. and Hwang, Y.C., “Introduction to Random Signals and Applied Kalman Filtering,” 3rd Ed., John Wiley & Sons, Inc. 1997.

Appendices

Appendix A

Detailed Test Results

Both Ranges	Error	Bias				Position							
Linear		TCAS		ADS-B		East		North		Alt		Avg Pos	
	Model	Avg	Std Dev	Avg	Std Dev	Avg	Std Dev	Avg	Std Dev	Avg	Std Dev	Avg	Std Dev
	ADS-B Only	N/A	N/A	N/A	N/A	16.3418	20.64	16.9397	20.83	21.9113	27.7	18.3976	40.33842
	Orig	2.5886	2.836	9.4824	46.69	4.7906	6.097	4.1922	5.717	6.0788	6.21	5.020533	10.41257
	Delay	2.5883	2.841	9.4822	46.69	4.7972	6.106	4.1923	5.718	5.9206	6.19	4.970033	10.40648
	Accel	2.5873	2.843	9.4827	46.69	4.7875	6.086	4.1814	5.697	5.894	6.159	4.9543	10.36477

Both Ranges	Error	Bias				Position							
Circle		TCAS		ADS-B		East		North		Alt		Avg Pos	
	Model	Avg	Std Dev	Avg	Std Dev	Avg	Std Dev	Avg	Std Dev	Avg	Std Dev	Avg	Std Dev
	ADS-B Only	N/A	N/A	N/A	N/A	16.3418	20.64	16.9397	20.83	21.9113	27.7	18.3976	40.33842
	Orig	2.8175	3.021	8.8494	46.55	11.9941	13.85	13.3894	15.13	16.4421	17.72	13.94187	27.10605
	Delay	2.8329	3.14	8.8504	46.55	11.9227	13.78	13.3972	15.14	16.3589	17.8	13.89293	27.12836
	Accel	1.9638	2.964	9.5647	46.64	5.5279	7.13	4.4633	5.851	5.6326	6.336	5.207933	11.19

Figure A.1: Detailed Test Results with ADS-B and TCAS Ranges

Both Ranges	Error	Rate								Accel							
Linear		East		North		Alt		Avg Vel		East		North		Alt		Avg Accel	
	Model	Avg	Std Dev	Avg	Std Dev	Avg	Std Dev	Avg	Std Dev	Avg	Std Dev	Avg	Std Dev	Avg	Std Dev	Avg	Std Dev
	ADS-B Only	0.5103	0.6411	0.643	0.8124	0.1868	0.2442	0.4467	1.063314	0.7535	0.9189	0.9042	1.145	0.2411	0.2975	0.632933	1.497968
	Orig	0.3482	0.4288	0.3292	0.405	0.1989	0.2442	0.2921	0.638379	N/A	N/A	N/A	N/A	N/A	N/A	N/A	N/A
	Delay	0.36	0.4447	0.3293	0.4051	0.1984	0.2432	0.2959	0.648853	N/A	N/A	N/A	N/A	N/A	N/A	N/A	N/A
	Accel	0.4557	0.5589	0.4539	0.5579	0.216	0.2672	0.3752	0.833677	0.1487	0.1938	0.1651	0.215	0.0696	0.08743	0.1278	0.30237

Both Ranges	Error	Rate								Accel							
Circle		East		North		Alt		Avg Vel		East		North		Alt		Avg Accel	
	Model	Avg	Std Dev	Avg	Std Dev	Avg	Std Dev	Avg	Std Dev	Avg	Std Dev	Avg	Std Dev	Avg	Std Dev	Avg	Std Dev
	ADS-B Only	0.639	0.8445	0.4122	0.5675	0.1868	0.2282	0.412667	1.042742	0.9393	1.274	0.5722	0.7947	0.2926	0.6343	0.601367	1.630019
	Orig	8.3657	9.43	8.7042	9.692	8.2254	9.184	8.431767	16.34643	N/A	N/A	N/A	N/A	N/A	N/A	N/A	N/A
	Delay	8.3426	9.405	8.704	9.691	8.223	9.181	8.4232	16.32974	N/A	N/A	N/A	N/A	N/A	N/A	N/A	N/A
	Accel	0.7674	0.9458	0.6267	0.7968	0.5996	0.7	0.664567	1.421066	0.5471	0.8049	0.4582	0.5332	0.5105	0.7758	0.505267	1.23856

Figure A.2: Detailed Test Results with ADS-B and TCAS Ranges

TCAS range only	Error	Bias				Position							
Linear		TCAS		ADS-B		East		North		Alt		Avg Pos	
	Model	Avg	Std Dev	Avg	Std Dev	Avg	Std Dev	Avg	Std Dev	Avg	Std Dev	Avg	Std Dev
	ADS-B Only	N/A	N/A	N/A	N/A	16.3418	20.64	16.9397	20.83	21.9113	27.7	18.3976	40.33842
	Orig	2.5804	2.863	N/A	N/A	4.7428	6.07	4.1536	5.698	6.0783	6.211	4.991567	10.38694
	Delay	2.58	2.868	N/A	N/A	4.7493	6.079	4.1539	5.699	5.9207	6.192	4.9413	10.38141
	Accel	2.5791	2.87	N/A	N/A	4.7453	6.059	4.1383	5.677	5.8942	6.16	4.925933	10.33854

TCAS range only	Error	Bias				Position							
Circle		TCAS		ADS-B		East		North		Alt		Avg Pos	
	Model	Avg	Std Dev	Avg	Std Dev	Avg	Std Dev	Avg	Std Dev	Avg	Std Dev	Avg	Std Dev
	ADS-B Only	N/A	N/A	N/A	N/A	16.3418	20.64	16.9397	20.83	21.9113	27.7	18.3976	40.33842
	Orig	2.8146	3.062	N/A	N/A	12.0668	13.9	13.398	15.15	16.4259	17.72	13.96357	27.14279
	Delay	2.8299	3.184	N/A	N/A	11.9957	13.83	13.4058	15.15	16.3519	17.81	13.9178	27.16593
	Accel	1.9681	3.008	N/A	N/A	5.4746	7.085	4.453	5.838	5.6589	6.346	5.1955	11.16025

Figure A.3: Detailed Test Results with Only TCAS Range

TCAS range only	Error	Rate								Accel							
Linear		East		North		Alt		Avg Vel		East		North		Alt		Avg Accel	
	Model	Avg	Std Dev	Avg	Std Dev	Avg	Std Dev	Avg	Std Dev	Avg	Std Dev	Avg	Std Dev	Avg	Std Dev	Avg	Std Dev
	ADS-B Only	0.5103	0.6411	0.643	0.8124	0.1868	0.2442	0.4467	1.063314	0.7535	0.9189	0.9042	1.145	0.2411	0.2975	0.632933	1.497968
	Orig	0.3463	0.4274	0.326	0.4016	0.1989	0.2442	0.2904	0.635285	N/A	N/A	N/A	N/A	N/A	N/A	N/A	N/A
	Delay	0.3588	0.4432	0.3261	0.4017	0.1984	0.2433	0.294433	0.645743	N/A	N/A	N/A	N/A	N/A	N/A	N/A	N/A
	Accel	0.4542	0.5573	0.4519	0.555	0.216	0.2673	0.374033	0.830697	0.1479	0.1932	0.1645	0.2144	0.0697	0.08744	0.127367	0.301562

TCAS range only	Error	Rate								Accel							
Circle		East		North		Alt		Avg Vel		East		North		Alt		Avg Accel	
	Model	Avg	Std Dev	Avg	Std Dev	Avg	Std Dev	Avg	Std Dev	Avg	Std Dev	Avg	Std Dev	Avg	Std Dev	Avg	Std Dev
	ADS-B Only	0.639	0.8445	0.4122	0.5675	0.1868	0.2282	0.412667	1.042742	0.9393	1.274	0.5722	0.7947	0.2926	0.6343	0.601367	1.630019
	Orig	8.3695	9.432	8.7055	9.693	8.225	9.184	8.433333	16.34817	N/A	N/A	N/A	N/A	N/A	N/A	N/A	N/A
	Delay	8.3464	9.408	8.7052	9.692	8.2226	9.181	8.424733	16.33206	N/A	N/A	N/A	N/A	N/A	N/A	N/A	N/A
	Accel	0.7644	0.9427	0.6259	0.7963	0.5984	0.6991	0.6629	1.41828	0.547	0.8048	0.4583	0.5331	0.5107	0.7759	0.505333	1.238515

Figure A.4: Detailed Test Results with Only TCAS Range

ADSB range only	Error	Bias				Position							
Linear		TCAS		ADS-B		East		North		Alt		Avg Pos	
	Model	Avg	Std Dev	Avg	Std Dev	Avg	Std Dev	Avg	Std Dev	Avg	Std Dev	Avg	Std Dev
	ADS-B Only	N/A	N/A	N/A	N/A	16.3418	20.64	16.9397	20.83	21.9113	27.7	18.3976	40.33842
	Orig	N/A	N/A	9.4829	46.69	5.4335	7.022	4.7947	5.83	6.1056	6.212	5.4446	11.04021
	Delay	N/A	N/A	9.4827	46.69	5.4379	7.031	4.7947	5.83	5.946	6.194	5.392867	11.03583
	Accel	N/A	N/A	9.483	46.69	5.4179	6.993	4.7899	5.812	5.9201	6.163	5.375967	10.98471

ADSB range only	Error	Bias				Position							
Circle		TCAS		ADS-B		East		North		Alt		Avg Pos	
	Model	Avg	Std Dev	Avg	Std Dev	Avg	Std Dev	Avg	Std Dev	Avg	Std Dev	Avg	Std Dev
	ADS-B Only	N/A	N/A	N/A	N/A	16.3418	20.64	16.9397	20.83	21.9113	27.7	18.3976	40.33842
	Orig	N/A	N/A	8.8689	46.55	12.0284	13.97	14.3975	15.99	17.2043	18.48	14.5434	28.14874
	Delay	N/A	N/A	8.8717	46.56	11.9577	13.9	14.3979	15.99	17.1138	18.54	14.4898	28.15354
	Accel	N/A	N/A	9.6734	46.64	5.5724	7.209	4.5871	5.876	6.0191	6.433	5.392867	11.30843

Figure A.5: Detailed Test Results with Only ADS-B Range

ADSB range only	Error	Rate								Accel							
Linear		East		North		Alt		Avg Vel		East		North		Alt		Avg Accel	
	Model	Avg	Std Dev	Avg	Std Dev	Avg	Std Dev	Avg	Std Dev	Avg	Std Dev	Avg	Std Dev	Avg	Std Dev	Avg	Std Dev
	ADS-B Only	0.5103	0.6411	0.643	0.8124	0.1868	0.2442	0.4467	1.063314	0.7535	0.9189	0.9042	1.145	0.2411	0.2975	0.632933	1.497968
	Orig	0.3119	0.395	0.3111	0.3879	0.1983	0.244	0.273767	0.605002	N/A	N/A	N/A	N/A	N/A	N/A	N/A	N/A
	Delay	0.3275	0.4134	0.3111	0.3879	0.1979	0.2431	0.278833	0.616817	N/A	N/A	N/A	N/A	N/A	N/A	N/A	N/A
	Accel	0.4194	0.5152	0.4343	0.5347	0.2164	0.2674	0.3567	0.789201	0.1462	0.1935	0.1603	0.2093	0.695	0.08739	0.333833	0.298137

ADSB range only	Error	Rate								Accel							
Circle		East		North		Alt		Avg Vel		East		North		Alt		Avg Accel	
	Model	Avg	Std Dev	Avg	Std Dev	Avg	Std Dev	Avg	Std Dev	Avg	Std Dev	Avg	Std Dev	Avg	Std Dev	Avg	Std Dev
	ADS-B Only	0.639	0.8445	0.4122	0.5675	0.1868	0.2282	0.412667	1.042742	0.9393	1.274	0.5722	0.7947	0.2926	0.6343	0.601367	1.630019
	Orig	8.4265	9.497	8.7881	9.777	8.2732	9.243	8.495933	16.46863	N/A	N/A	N/A	N/A	N/A	N/A	N/A	N/A
	Delay	8.4011	9.471	8.788	9.777	8.2706	9.24	8.486567	16.45197	N/A	N/A	N/A	N/A	N/A	N/A	N/A	N/A
	Accel	0.7657	0.9399	0.613	0.7682	0.599	0.6887	0.659233	1.395654	0.5424	0.803	0.4546	0.5278	0.5095	0.7763	0.502167	1.235323

Figure A.6: Detailed Test Results with Only ADS-B Range

No Ranges	Error	Bias				Position							
Linear		TCAS		ADS-B		East		North		Alt		Avg Pos	
	Model	Avg	Std Dev	Avg	Std Dev	Avg	Std Dev	Avg	Std Dev	Avg	Std Dev	Avg	Std Dev
	ADS-B Only	N/A	N/A	N/A	N/A	16.3418	20.64	16.9397	20.83	21.9113	27.7	18.3976	40.33842
	Orig	N/A	N/A	N/A	N/A	5.49	7.073	4.7197	5.784	6.1053	6.215	5.438333	11.05026
	Delay	N/A	N/A	N/A	N/A	5.4954	7.081	4.7197	5.784	5.9465	6.197	5.3872	11.04527
	Accel	N/A	N/A	N/A	N/A	5.4734	7.042	4.7149	5.765	5.9206	6.166	5.369633	10.99293

No Ranges	Error	Bias				Position							
Circle		TCAS		ADS-B		East		North		Alt		Avg Pos	
	Model	Avg	Std Dev	Avg	Std Dev	Avg	Std Dev	Avg	Std Dev	Avg	Std Dev	Avg	Std Dev
	ADS-B Only	N/A	N/A	N/A	N/A	16.3418	20.64	16.9397	20.83	21.9113	27.7	18.3976	40.33842
	Orig	N/A	N/A	N/A	N/A	12.1602	14.08	14.4751	16.05	17.1748	18.49	14.60337	28.2441
	Delay	N/A	N/A	N/A	N/A	12.0876	14.01	14.475	16.05	17.0933	18.56	14.55197	28.2552
	Accel	N/A	N/A	N/A	N/A	5.498	7.133	4.612	5.871	6.0808	6.43	5.396933	11.25581

Figure A.7: Detailed Test Results with No Range Data

No Ranges	Error	Rate								Accel							
Linear		East		North		Alt		Avg Vel		East		North		Alt		Avg Accel	
	Model	Avg	Std Dev	Avg	Std Dev	Avg	Std Dev	Avg	Std Dev	Avg	Std Dev	Avg	Std Dev	Avg	Std Dev	Avg	Std Dev
	ADS-B Only	0.5103	0.6411	0.643	0.8124	0.1868	0.2442	0.4467	1.063314	0.7535	0.9189	0.9042	1.145	0.2411	0.2975	0.632933	1.497968
	Orig	0.3122	0.3956	0.3082	0.3819	0.1983	0.244	0.2729	0.601567	N/A	N/A	N/A	N/A	N/A	N/A	N/A	N/A
	Delay	0.3275	0.4139	0.3083	0.3819	0.1979	0.2431	0.2779	0.613399	N/A	N/A	N/A	N/A	N/A	N/A	N/A	N/A
	Accel	0.4195	0.5149	0.4298	0.5303	0.2165	0.2674	0.355267	0.78603	0.1457	0.1935	0.1595	0.2087	0.0696	0.0874	0.124933	0.297719

No Ranges	Error	Rate								Accel							
Circle		East		North		Alt		Avg Vel		East		North		Alt		Avg Accel	
	Model	Avg	Std Dev	Avg	Std Dev	Avg	Std Dev	Avg	Std Dev	Avg	Std Dev	Avg	Std Dev	Avg	Std Dev	Avg	Std Dev
	ADS-B Only	0.639	0.8445	0.4122	0.5675	0.1868	0.2282	0.412667	1.042742	0.9393	1.274	0.5722	0.7947	0.2926	0.6343	0.601367	1.630019
	Orig	8.4323	9.501	8.7901	9.779	8.2726	9.243	8.498333	16.47212	N/A	N/A	N/A	N/A	N/A	N/A	N/A	N/A
	Delay	8.4067	9.475	8.79	9.779	8.27	9.24	8.4889	16.45546	N/A	N/A	N/A	N/A	N/A	N/A	N/A	N/A
	Accel	0.7608	0.9359	0.6132	0.7677	0.5979	0.6875	0.6573	1.392095	0.5426	0.8031	0.4546	0.5276	0.5098	0.7764	0.502333	1.235366

Figure A.8: Detailed Test Results with No Range Data

15% Msg Loss	Error	Bias				Position							
Linear		TCAS		ADS-B		East		North		Alt		Avg Pos	
	Model	Avg	Std Dev	Avg	Std Dev	Avg	Std Dev	Avg	Std Dev	Avg	Std Dev	Avg	Std Dev
	ADS-B Only	N/A	N/A	N/A	N/A	16.3418	20.64	16.9397	20.83	21.9113	27.7	18.3976	40.33842
	Orig	2.3477	3.011	11.64	47.24	5.4154	6.738	4.9025	6.474	5.5714	6.145	5.296433	11.18366
	Delay	2.3464	3.009	11.656	47.24	5.3611	6.817	4.9395	6.539	5.4244	6.081	5.241667	11.23426
	Accel	9.1952	11.16	13.035	47.8	49.36	78.07	49.9949	80.87	5.156	6.327	34.83697	112.5829

15% Msg Loss	Erorr	Bias				Position							
Circle		TCAS		ADS-B		East		North		Alt		Avg Pos	
	Model	Avg	Std Dev	Avg	Std Dev	Avg	Std Dev	Avg	Std Dev	Avg	Std Dev	Avg	Std Dev
	ADS-B Only	N/A	N/A	N/A	N/A	16.3418	20.64	16.9397	20.83	21.9113	27.7	18.3976	40.33842
	Orig	2.9809	2.897	11.251	47.12	15.2308	17.59	17.7071	22.49	20.1081	22.67	17.682	36.45733
	Delay	2.9977	2.952	11.26	47.13	15.108	17.46	17.5708	22.45	19.6592	22.4	17.446	36.2024
	Accel	9.2959	11.8	13.315	47.69	45.1643	76.55	34.0014	49.1	39.3198	69.35	39.49517	114.3684

Figure A.9: Detailed Test Results with 15% Message Loss

15% Msg Loss	Error	Rate								Accel							
Linear		East		North		Alt		Avg Vel		East		North		Alt		Avg Accel	
	Model	Avg	Std Dev	Avg	Std Dev	Avg	Std Dev	Avg	Std Dev	Avg	Std Dev	Avg	Std Dev	Avg	Std Dev	Avg	Std Dev
	ADS-B Only	0.5103	0.6411	0.643	0.8124	0.1868	0.2442	0.4467	1.063314	0.7535	0.9189	0.9042	1.145	0.2411	0.2975	0.632933	1.497968
	Orig	0.3617	0.4468	0.3519	0.4336	0.2211	0.2764	0.311567	0.681202	N/A	N/A	N/A	N/A	N/A	N/A	N/A	N/A
	Delay	0.4061	0.501	0.3542	0.4352	0.2207	0.2748	0.327	0.718272	N/A	N/A	N/A	N/A	N/A	N/A	N/A	N/A
	Accel	2.2096	3.99	2.3121	5.391	0.2764	0.3554	1.599367	6.716345	1.1301	1.685	1.0879	1.625	0.0922	0.1104	0.770067	2.34351

15% Msg Loss	Erorr	Rate								Accel							
Circle		East		North		Alt		Avg Vel		East		North		Alt		Avg Accel	
	Model	Avg	Std Dev	Avg	Std Dev	Avg	Std Dev	Avg	Std Dev	Avg	Std Dev	Avg	Std Dev	Avg	Std Dev	Avg	Std Dev
	ADS-B Only	0.639	0.8445	0.4122	0.5675	0.1868	0.2282	0.412667	1.042742	0.9393	1.274	0.5722	0.7947	0.2926	0.6343	0.601367	1.630019
	Orig	9.4472	10.67	10.2297	12.05	9.616	11	9.7643	19.49491	N/A	N/A	N/A	N/A	N/A	N/A	N/A	N/A
	Delay	9.4107	10.63	10.2123	12.03	9.574	10.95	9.732333	19.43245	N/A	N/A	N/A	N/A	N/A	N/A	N/A	N/A
	Accel	2.7511	7.097	1.4328	2.407	1.8362	4.124	2.0067	8.553855	1.0592	1.715	0.655	0.8632	0.759	1.195	0.8244	2.261496

Figure A.10: Detailed Test Results with 15% Message Loss

No-Delay EKF Tuning	Error	Bias				Position							
Linear		TCAS		ADS-B		East		North		Alt		Avg Pos	
	Model	Avg	Std Dev	Avg	Std Dev	Avg	Std Dev	Avg	Std Dev	Avg	Std Dev	Avg	Std Dev
	ADS-B Only	N/A	N/A	N/A	N/A	16.3418	20.64	16.9397	20.83	21.9113	27.7	18.3976	40.33842
	0.5G	2.5886	2.836	9.4824	46.69	4.7906	6.097	4.1922	5.717	6.0788	6.21	5.020533	10.41257
	2G	2.5831	2.842	9.4844	46.69	4.9788	6.303	4.3759	5.939	6.3009	6.53	5.218533	10.84622
	3.5G	2.5775	2.85	9.4866	46.69	5.2852	6.655	4.7257	6.354	6.6993	7.1	5.570067	11.62206
	5G	2.5761	2.859	9.4881	46.69	5.6394	7.077	5.1304	6.86	7.2123	7.762	5.994033	12.5456
	10G	2.5937	2.884	9.4856	46.69	6.7933	8.568	6.4309	8.574	9.0675	9.921	7.430567	15.66366

No-Delay EKF Tuning	Error	Bias				Position							
Circle		TCAS		ADS-B		East		North		Alt		Avg Pos	
	Model	Avg	Std Dev	Avg	Std Dev	Avg	Std Dev	Avg	Std Dev	Avg	Std Dev	Avg	Std Dev
	ADS-B Only	N/A	N/A	N/A	N/A	16.3418	20.64	16.9397	20.83	21.9113	27.7	18.3976	40.33842
	0.5G	2.8175	3.021	8.8494	46.55	11.9941	13.85	13.3894	15.13	16.4421	17.72	13.94187	27.10605
	2G	1.9481	2.834	9.5244	46.63	5.5822	7.156	4.6281	6.054	6.2608	7.043	5.490367	11.72447
	3.5G	1.9479	2.845	9.5318	46.63	6.0835	7.77	5.0317	6.558	6.4338	7.331	5.849667	12.5349
	5G	1.9571	2.845	9.5213	46.63	6.5301	8.295	5.4624	7.133	6.9108	7.899	6.3011	13.49374
	10G	1.909	2.765	9.5305	46.62	7.8318	9.791	6.8633	8.94	8.7558	9.902	7.816967	16.54802

Figure A.11: Detailed Test Results for EKF Tuning

No-Delay EKF Tuning	Error	Rate							
Linear		East		North		Alt		Avg Vel	
	Model	Avg	Std Dev	Avg	Std Dev	Avg	Std Dev	Avg	Std Dev
	ADS-B Only	0.5103	0.6411	0.643	0.8124	0.1868	0.2442	0.4467	1.063314
	0.5G	0.3482	0.4288	0.3292	0.405	0.1989	0.2442	0.2921	0.638379
	2G	0.4554	0.5668	0.5464	0.6732	0.1938	0.2453	0.398533	0.913582
	3.5G	0.4947	0.6178	0.6033	0.7518	0.1996	0.2526	0.432533	1.005329
	5G	0.5082	0.6361	0.6239	0.7808	0.2018	0.2548	0.444633	1.038843
	10G	0.5145	0.6474	0.6408	0.8055	0.2021	0.2532	0.452467	1.063986

No-Delay EKF Tuning	Error	Rate							
Circle		East		North		Alt		Avg Vel	
	Model	Avg	Std Dev	Avg	Std Dev	Avg	Std Dev	Avg	Std Dev
	ADS-B Only	0.639	0.8445	0.4122	0.5675	0.1868	0.2282	0.412667	1.042742
	0.5G	8.3657	9.43	8.7042	9.692	8.2254	9.184	8.431767	16.34643
	2G	1.2999	1.487	1.3546	1.52	1.1987	1.347	1.2844	2.517137
	3.5G	0.7247	0.9067	0.666	0.7952	0.4872	0.569	0.625967	1.333495
	5G	0.6412	0.8388	0.5141	0.6542	0.3036	0.3727	0.4863	1.127151
	10G	0.6358	0.8362	0.4396	0.5957	0.211	0.2643	0.4288	1.060162

Figure A.12: Detailed Test Results for EKF Tuning

Range Comparison	Error	Bias				Position							
Linear		TCAS		ADS-B		East		North		Alt		Avg Pos	
	Model	Avg	Std Dev	Avg	Std Dev	Avg	Std Dev	Avg	Std Dev	Avg	Std Dev	Avg	Std Dev
	ADS-B Only	N/A	N/A	N/A	N/A	16.3418	20.64	16.9397	20.83	21.9113	27.7	18.3976	40.33842
	Both	2.5775	2.85	9.4866	46.69	5.2852	6.655	4.7257	6.354	6.6993	7.1	5.570067	11.62206
	TCAS Only	2.5707	2.876	N/A	N/A	5.2523	6.627	4.6939	6.339	6.6994	7.102	5.548533	11.59907
	ADS-B Only	N/A	N/A	9.4841	46.69	6.1149	7.831	5.3799	6.542	6.7204	7.102	6.071733	12.43225
	None	N/A	N/A	N/A	N/A	6.1607	7.906	5.2966	6.496	6.7212	7.105	6.0595	12.45728

Range Comparison	Error	Bias				Position							
Circle		TCAS		ADS-B		East		North		Alt		Avg Pos	
	Model	Avg	Std Dev	Avg	Std Dev	Avg	Std Dev	Avg	Std Dev	Avg	Std Dev	Avg	Std Dev
	ADS-B Only	N/A	N/A	N/A	N/A	16.3418	20.64	16.9397	20.83	21.9113	27.7	18.3976	40.33842
	Both	1.9479	2.845	9.5318	46.63	6.0835	7.77	5.0317	6.558	6.4338	7.331	5.849667	12.5349
	TCAS Only	1.9513	2.884	N/A	N/A	6.0479	7.733	5.0146	6.538	6.46	7.336	5.840833	12.50446
	ADS-B Only	N/A	N/A	9.6293	46.63	6.1724	7.955	5.231	6.611	6.8583	7.391	6.087233	12.71276
	None	N/A	N/A	N/A	N/A	6.0907	7.888	5.2486	6.598	6.902	7.381	6.080433	12.65833

Figure A.13: Detailed Range Measurement Comparison

Range Comparison	Error	Rate							
Linear		East		North		Alt		Avg Vel	
	Model	Avg	Std Dev	Avg	Std Dev	Avg	Std Dev	Avg	Std Dev
	ADS-B Only	0.5103	0.6411	0.643	0.8124	0.1868	0.2442	0.4467	1.063314
	Both	0.4947	0.6178	0.6033	0.7518	0.1996	0.2526	0.432533	1.005329
	TCAS Only	0.4954	0.619	0.604	0.7514	0.1996	0.2526	0.433	1.005768
	ADS-B Only	0.4783	0.6044	0.5884	0.7396	0.1996	0.2524	0.4221	0.987934
	None	0.478	0.606	0.5879	0.7388	0.1995	0.2524	0.4218	0.988315

Range Comparison	Error	Rate							
Circle		East		North		Alt		Avg Vel	
	Model	Avg	Std Dev	Avg	Std Dev	Avg	Std Dev	Avg	Std Dev
	ADS-B Only	0.639	0.8445	0.4122	0.5675	0.1868	0.2282	0.412667	1.042742
	Both	0.7247	0.9067	0.666	0.7952	0.4872	0.569	0.625967	1.333495
	TCAS Only	0.724	0.9062	0.6664	0.795	0.4866	0.5688	0.625667	1.33295
	ADS-B Only	0.7243	0.9038	0.6595	0.776	0.4901	0.5678	0.624633	1.319631
	None	0.7243	0.903	0.6597	0.7756	0.4898	0.5673	0.6246	1.318633

Figure A.14: Detailed Range Measurement Comparison

No-Delay EKF vs ADS-B	Error	Bias				Position							
Linear		TCAS		ADS-B		East		North		Alt		Avg Pos	
	Model	Avg	Std Dev	Avg	Std Dev	Avg	Std Dev	Avg	Std Dev	Avg	Std Dev	Avg	Std Dev
	ADS-B Only	N/A	N/A	N/A	N/A	16.3418	20.64	16.9397	20.83	21.9113	27.7	18.3976	40.33842
	No Message Loss	2.5707	2.876	N/A	N/A	5.2523	6.627	4.6939	6.339	6.6994	7.102	5.548533	11.59907
	15% Message loss	2.3331	3.035	N/A	N/A	6.1791	7.662	5.7708	7.479	6.6346	7.806	6.194833	13.25048

No-Delay EKF vs ADS-B	Error	Bias				Position							
Circle		TCAS		ADS-B		East		North		Alt		Avg Pos	
	Model	Avg	Std Dev	Avg	Std Dev	Avg	Std Dev	Avg	Std Dev	Avg	Std Dev	Avg	Std Dev
	ADS-B Only	N/A	N/A	N/A	N/A	16.3418	20.64	16.9397	20.83	21.9113	27.7	18.3976	40.33842
	No Message Loss	1.9513	2.884	N/A	N/A	6.0479	7.733	5.0146	6.538	6.46	7.336	5.840833	12.50446
	15% Message Loss	1.7648	2.579	N/A	N/A	7.1133	8.917	6.698	8.917	6.4327	7.804	6.748	14.82998

Figure A.15: Detailed No-Delay EKF Comparison to ADS-B Unprocessed Report

Range Comparison	Error	Rate							
Linear		East		North		Alt		Avg Vel	
	Model	Avg	Std Dev	Avg	Std Dev	Avg	Std Dev	Avg	Std Dev
	ADS-B Only	0.5103	0.6411	0.643	0.8124	0.1868	0.2442	0.4467	1.063314
	Both	0.4947	0.6178	0.6033	0.7518	0.1996	0.2526	0.432533	1.005329
	TCAS Only	0.4954	0.619	0.604	0.7514	0.1996	0.2526	0.433	1.005768
	ADS-B Only	0.4783	0.6044	0.5884	0.7396	0.1996	0.2524	0.4221	0.987934
	None	0.478	0.606	0.5879	0.7388	0.1995	0.2524	0.4218	0.988315

Range Comparison	Error	Rate							
Circle		East		North		Alt		Avg Vel	
	Model	Avg	Std Dev	Avg	Std Dev	Avg	Std Dev	Avg	Std Dev
	ADS-B Only	0.639	0.8445	0.4122	0.5675	0.1868	0.2282	0.412667	1.042742
	Both	0.7247	0.9067	0.666	0.7952	0.4872	0.569	0.625967	1.333495
	TCAS Only	0.724	0.9062	0.6664	0.795	0.4866	0.5688	0.625667	1.33295
	ADS-B Only	0.7243	0.9038	0.6595	0.776	0.4901	0.5678	0.624633	1.319631
	None	0.7243	0.903	0.6597	0.7756	0.4898	0.5673	0.6246	1.318633

Figure A.16: Detailed No-Delay EKF Comparison to ADS-B Unprocessed Report